Development 137, 2237-2250 (2010) doi:10.1242/dev.049692

Nuclear pre-mRNA 3′-end processing regulates synapse and axon development in *C. elegans*

Heather Van Epps[1,*], Ya Dai[2,†], Yingchuan Qi[1], Alexandr Goncharov[1,2] and Yishi Jin[1,2,‡]

SUMMARY

Nuclear pre-mRNA 3′-end processing is vital for the production of mature mRNA and the generation of the 3′ untranslated region (UTR). However, the roles and regulation of this event in cellular development remain poorly understood. Here, we report the function of a nuclear pre-mRNA 3′-end processing pathway in synapse and axon formation in *C. elegans*. In a genetic enhancer screen for synaptogenesis mutants, we identified a novel polyproline-rich protein, Synaptic defective enhancer-1 (SYDN-1). Loss of function of *sydn-1* causes abnormal synapse and axon development, and displays striking synergistic interactions with several genes that regulate specific aspects of synapses. SYDN-1 is required in neurons and localizes to distinct regions of the nucleus. Through a genetic suppressor screen, we found that the neuronal defects of *sydn-1* mutants are suppressed by loss of function in Polyadenylation factor subunit-2 (PFS-2), a conserved WD40-repeat protein that interacts with multiple subcomplexes of the pre-mRNA 3′-end processing machinery. PFS-2 partially colocalizes with SYDN-1, and SYDN-1 influences the nuclear abundance of PFS-2. Inactivation of several members of the nuclear 3′-end processing complex suppresses *sydn-1* mutants. Furthermore, lack of *sydn-1* can increase the activity of 3′-end processing. Our studies provide in vivo evidence for pre-mRNA 3′-end processing in synapse and axon development and identify SYDN-1 as a negative regulator of this cellular event in neurons.

KEY WORDS: Synapse, Axon development, Pre-mRNA 3′-end processing, Nuclear polyadenylation, *C. elegans*

INTRODUCTION

Nuclear processing of the 3′ end of pre-mRNA is crucial for the generation of the 3′ untranslated region (UTR), mRNA maturation and subsequent export into the cytoplasm (Mandel et al., 2008). This pre-mRNA processing event entails multi-step reactions defined as sequence recognition, cleavage, and the addition of a polyadenine tail at the 3′ end, collectively referred to as nuclear polyadenylation (NpolyA). NpolyA activities require a megadalton protein complex that acts on pre-mRNA cis-regulatory elements. In mammalian cells, catalysis of 3′ cleavage requires cleavage and polyadenylation specificity factor 73 (CPSF-73; CPSF3), and polyadenylation is catalyzed by polyA polymerase (PAP). These core proteins are components of a much larger polyadenylation machinery that includes four major subcomplexes: Cleavage factor I (CFI), Cleavage factor II (CFII), Cleavage and polyadenylation specificity factor (CPSF) and Cleavage stimulation factor (CstF) (Mandel et al., 2008; Shi et al., 2009). These subcomplexes act in concert to control the recognition, specificity and activity of the NpolyA process, which also coordinates with transcription and splicing (Moore and Proudfoot, 2009). Constitutive NpolyA is essential for cell viability and growth (Bloch et al., 1978; Maftahi et al., 1998; Ohnacker et al., 2000; Wang et al., 2005; Xu et al., 2006; Zhao et al., 1999). Both loss- and gain-of-function alterations in cis and trans factors in NpolyA lead to a variety of diseases, including thrombophilia, thalassemias, cancer and muscular dystrophy (Danckwardt et al., 2008; Mayr and Bartel, 2009).

Recently, genome-wide RNA analyses have revealed that extensive regulation must occur at the 3′ ends of pre-mRNA. In human tissues, it is estimated over 50% of transcripts have alternative 3′ terminal exons, 3′ UTRs and polyadenylation sites (Wang et al., 2008). Regulation via alternative NpolyA can be particularly prevalent in the nervous system. For example, isoforms of neuronal proteins that differ as the result of alternative polyadenylation, such as Homer1, can be rapidly produced in an activity-dependent manner (Flavell et al., 2008; Niibori et al., 2007). The neuronal RNA-binding protein Nova shows preferential binding at the 3′ ends and regulates alternative polyadenylation of many transcripts (Licatalosi et al., 2008). However, the trans-acting regulators of pre-mRNA 3′-end processing and their roles in specific cellular and developmental processes remain poorly understood.

Here, using genetic modifier screens in *C. elegans*, we have uncovered a role of the novel protein SYDN-1 and the NpolyA processing factor PFS-2 in neuronal development. The PFS2 (Polyadenylation factor subunit 2) protein family is characterized by the presence of seven highly conserved WD repeats (Smith et al., 1999), and was originally identified from yeast and mammalian cells based on the polyadenylation activity (Preker et al., 1997; Shi et al., 2009). Yeast Pfs2p directly interacts with proteins in subcomplexes of NpolyA and possibly acts as a scaffold for the 3′-end processing machinery (Ohnacker et al., 2000). Yeast Pfs2p is essential for viability. By contrast, an *Arabidopsis* PFS2 protein, FY, is dispensable for cell viability and controls floral timing (Simpson et al., 2003; Xu et al., 2006). These observations suggest that PFS2 proteins are involved not only in constitutive NpolyA, but also in specific regulatory processes. We find that loss of function of *sydn-1* disrupts axon and synapse morphology in *C.*

[1]Division of Biological Sciences, Section of Neurobiology, University of California, San Diego, CA 92093, USA. [2]Howard Hughes Medical Institute, 4000 Jones Bridge Road, Chevy Chase, MD 20815-6789, USA.

*Present address: Department of Biology, Western Washington University, Bellingham, WA 98225, USA
†Present address: Department of Pathology and Cell Biology, Columbia University Medical Center, New York, NY 10032, USA
‡Author for correspondence (yijin@ucsd.edu)

Accepted 27 April 2010

elegans, and that reduction of *pfs-2* and NpolyA activities restores these defects to normal. Our studies show that SYDN-1 is a negative regulator of NpolyA and support a conclusion that the activity levels of NpolyA are crucial for neuronal development in a context-dependent manner.

MATERIALS AND METHODS

C. elegans genetics

Strains were maintained as described (Brenner, 1974). For transgene, strain and allele information, see Table 1. All double mutants were constructed following standard procedures, and the genotypes were confirmed by allele-associated single-nucleotide polymorphisms (SNPs) using the primers listed in Table S1 in the supplementary material.

Enhancers were obtained by mutagenizing CZ455 *rpm-1(ju44);juIs1*[P_{unc-25}SNB-1::GFP] with 50 mM EMS. F2 progeny were first screened for severe uncoordination, followed by examination of the SNB-1::GFP-encoding transgene. Candidate mutants were backcrossed to N2 to confirm enhancement. We obtained 14 enhancer mutations from 20,000 haploid genomes, including seven *syd-2* alleles, four *sad-1* alleles and two *syd-1* alleles. *sydn-1(ju541)* defined a new locus.

Suppressors of *sydn-1* were isolated by mutagenizing CZ4767 *sydn-1(ju541);syd-2(ju37);juIs76*[P_{unc-25}GFP] with 50 mM EMS. Mutants that showed suppression of the Unc behavior, but retention of Syd-2 behavior, were further examined for suppression of *sydn-1* using P_{unc-25} GFP. We obtained ten suppressors from 10,000 haploid genomes.

The *ju541* and *ju608* mutations were mapped to chromosomes I and II, respectively, using SNPs between Hawaiian (CB4856) and N2 strains (Wicks et al., 2001) (Fig. 5A, Fig. 6A). We constructed the *dapk-1(ju4) sydn-1(ju541) dpy-5(e61);juIs1* strain to further map *ju541* between *snp_Y39G10AR[4]* and *snp_Y39G10AR[6]*, placing *ju541* in a 4 kb interval of the 5′ region of *Y39G10AR.17*. *ju608* was first mapped between *pas11767* and *pas43942* and to the left of *unc-52*.

Molecular biology and transgenic constructs

DNA manipulations followed standard procedures. Plasmids were generated using Gateway technology (Invitrogen, Carlsbad, CA, USA): pCZGY165(P_{dpy-7}SYDN-1(cDNA)), pCZGY147(P_{rgef-1}SYDN-1(cDNA)), pCZGY180(P_{rgef-1}FLAG::SYDN-1(cDNA)), pCZGY748(P_{unc-25}SYDN-1(cDNA)), pCZGY650(P_{pfs-2}PFS-2(genomic)::GFP), pCZGY754(P_{pfs-2} PFS-2(genomic)::mCHERRY). Germline transformation was performed following standard procedures (Mello et al., 1991), using 50-75 ng/μl P_{ttx-3}GFP or P_{ttx-3}RFP as a co-injection marker.

Axon and synapse morphology analysis

Transgenic GFP reporters in live animals were observed using a 63× Plan-Apochromat objective and Chroma filter sets on a Zeiss Axioplan2 microscope. Ectopic axon branches were quantitated as the number of neurons displaying branches divided by the number of neurons scored per animal. The complexity of ectopic branches always correlated with an increased total number of branches in a given animal. Confocal images of *juIs1*[P_{unc-25}SNB-1::GFP] were obtained from the central region of the dorsal nerve cords of 1-day-old adults using a 63× Plan-Apochromat objective. SNB-1::GFP *z*-stacks were constructed from four to eight 0.4 μm merged planes. *z*-stacks of SNB-1::GFP soma expression were constructed from nine to sixteen 0.4 μm merged planes of motoneuron cell bodies. Fluorescence intensity in the soma was determined using ImageJ (rsb.info.nih.gov/ij). A circle was drawn covering the entire soma and the average soma intensity minus background was calculated.

Immunostaining and image analysis

Whole-mount staining was conducted as described previously (Finney and Ruvkun, 1990). Samples were processed in parallel. Primary antibodies were: rabbit anti-FLAG (1:1000) and mouse anti-GFP (1:500) from Invitrogen; rabbit anti-ELKS-1 (1:500) and rabbit anti-SNT-1 (1:2000), gifts from Michael Nonet (Deken et al., 2005; Nonet et al., 1993); and rabbit anti-CPF-2 (1:500), a gift of Tom Blumenthal (Evans, 2001). DAPI stain and goat anti-rabbit Alexa Fluor 594 and goat anti-mouse Alexa Fluor 488 secondary antibodies were from Invitrogen.

Confocal images of immunostained PFS-2::GFP, FLAG::SYDN-1, ELKS-1 and SNT-1 were collected using a Plan-Apochromat 100× objective on a Zeiss LSM 500 or 700 microscope with 488 nm and 594 nm lasers. Laser output was set to 40% and transmission was optimized for minimum bleed-through and optimal detection. Detector gain was tuned to minimize pixel saturation and maximize detection range. Single 0.4 μm confocal planes were captured for each channel, merged using LSM software and exported as a TIFF file. The ELKS-1 immunostaining area, distance and intensity were calculated above threshold using the Region Measurement function of MetaMorph. Colocalization images of PFS-2::GFP and FLAG::SYDN-1 with DAPI were obtained using a 63× Plan-Apochromat objective and Chroma filter set on an Axioplan2 microscope and merged using Adobe Photoshop CS. For quantification of PFS-2::GFP and FLAG::SYDN-1, confocal *z*-stacks were constructed from six to fifteen 0.4 μm merged planes and analyzed using ImageJ.

RNA analysis

Total RNA was extracted from mixed-stage animals using Trizol and reverse transcribed using an oligo(dT) primer and SuperScript III First-Strand Synthesis System for RT-PCR according to the manufacturer's protocol (Invitrogen). We performed 5′ and 3′ RACE reactions using the 5′/3′ RACE Kit (Roche Applied Science, Indianapolis, IN, USA); for primers, see Table S1 in the supplementary material. No SL1 or SL2 splice leaders were detected in the 5′ RACE products. The full-length *sydn-1* cDNA was 2057 bp, starting from ATG through 320 bp of the 3′ UTR, and was confirmed by DNA sequence analysis.

Quantitative (q) RT-PCR was conducted using SYBR Green on a StepOne Real-Time PCR System, and data were analyzed using StepOne v2.1 (Applied Biosystems, Foster City, CA, USA). The normalized transcript levels were determined by first setting the threshold of product production below saturation, and then determining the cycle at which the threshold was met for each sample. The value for *lin-15A* transcripts was divided by that of *ama-1*. The ratio of *lin-15A* to *ama-1* was then normalized to that of the N2 strain. At least two different RNA samples were used per genotype.

RNA interference (RNAi)

A *pfs-2* RNAi plasmid (pCZGY649) was constructed by cloning 500 bp of *pfs-2* genomic DNA, amplified from cosmid R06A4, into pCZGY115 (equivalent to the L4440 vector). All other RNAi clones were obtained from the Ahringer Library (Geneservice, Cambridge, UK) (Fraser et al., 2000). Feeding RNAi was conducted as described (Kamath et al., 2001). For titrated *pfs-2* RNAi, overnight HT115 cultures expressing *pfs-2* double-stranded RNA were diluted 1:10 to 1:200 with HT115 culture. RNAi treatment was performed in triplicate and conducted in two independent experiments at 15°C.

Electron microscopy

A mixture of L4 to young adults from four strains – N2, CZ333 *juIs1*, CZ4574 *sydn-1(ju541);juIs1* and CZ4741 *sydn-1(ju541)* – were fixed following a high-pressure freeze procedure as described (Weimer et al., 2006). Sections (50 nm) were collected and imaged at 10,000× magnification on a JEOL-1200 EX transmission electron microscope fitted with a Gatan Orius SC600 digital camera. Axon measurements were collected from digital micrographs of ventral and dorsal nerve cords using ImageJ. Axon diameter was calculated from the longest cross-sectional axis.

lin-15 Muv phenotype scoring

Strains containing *lin-15(n765ts)* were maintained at 15°C. L1 larvae were shifted to 22.5°C in parallel. Three days later, adults were scored as Muv if they displayed one or more vulval protrusions. *sydn-1;lin-15(n765ts)* animals were 100% Muv, and the number of vulval protrusions was scored.

RESULTS

sydn-1 mutants show abnormal axon and synapse development

Complete loss of function in several synaptogenesis genes, such as *rpm-1*, *syd-2* and *syd-1*, leads to distinct defects in synapse development yet comparatively mild effects on the behavior of the

Table 1. Strains and transgenic lines

Strain	Genotype
Mutant strains	
CZ9714	*pfs-2(ju608)*
BW568	*lin-15(n765ts)*
CZ9809	*pfs-2(ju608);lin-15(ju608)*
VWL4	*sydn-1(ju541);lin-15(ju608)*
CZ4741	*sydn-1(ju541)*
CZ4738	*sydn-1(ju541);rpm-1(ju44)*
CZ4740	*sydn-1(ju541);syd-2(ju37)*
SYDN-1 expression strains	
CZ5594	*sydn-1(ju541);juIs1;juEx1074[Psydn-1SYDN-1(genomic)]*
CZ7129	*sydn-1(ju541);juIs76;juEx1376[Pdpy-7 SYDN-1(cDNA)]*
CZ7190	*sydn-1(ju541);juEx1387[Prgef-1 FLAG::SYDN-1(cDNA)]*
CZ9566	*pfs-2(ju608);juIs1;juEx1389[Prgef-1 FLAG::SYDN-1(cDNA)]*
CZ9567	*juIs1;juEx1389[Prgef-1 FLAG::SYDN-1(cDNA)]*
CZ9564	*sydn-1(ju541);juIs1;juEx1389[Prgef-1 FLAG::SYDN-1(cDNA)]*
CZ9568	*pfs-2(ju608);juEx1389[Prgef-1 FLAG::SYDN-1(cDNA)]*
CZ9562	*sydn-1(ju541);juIs1;juIs246[Prgef-1 FLAG::SYDN-1(cDNA)]*
CZ8715	*juIs246[Prgef-1 FLAG::SYDN-1(cDNA)]*
CZ8716	*sydn-1(ju541);juIs246[Prgef-1 FLAG::SYDN-1(cDNA)]*
CZ9523	*pfs-2(ju608);juIs246[Prgef-1 FLAG::SYDN-1(cDNA)];juIs1*
CZ9127	*sydn-1(ju541);juIs1;juEx1843[Punc-25SYDN-1(cDNA)]*
CZ9530	*sydn-1(ju541);juIs1;juEx1988[Psydn-1SYDN-1(lf)(genomic)]*
CZ9565	*juIs1;juEx1996[Psydn-1SYDN-1(lf)(genomic)]*
PFS-2 expression strains	
CZ8938	*sydn-1(ju541);pfs-2(ju608);syd-2(ju37);juIs76;juEx1755[Ppfs-2PFS-2)]*
CZ9107	*juEx1848[pfs-2(ju608)]*
CZ9394	*sydn-1(ju541);juEx1849[Ppfs-2PFS-2(plf)]*
CZ9563	*sydn-1(ju541);juIs1;juEx1850[Ppfs-2PFS-2(plf)]*
CZ9541	*sydn-1(ju541);pfs-2(ju608);syd-2(ju37);juIs76;juEx2001[Ppfs-2PFS-2::GFP]*
CZ9527	*juEx1991[Ppfs-2PFS-2::GFP,Prgef-1 FLAG::SYDN-1(cDNA)]*
CZ9546	*sydn-1(ju541);pfs-2(ju608);syd-2(ju37);juIs76;juEx2007[Ppfs-2PFS-2(WD domains)]*
CZ11654	*sydn-1(ju541);juEx1939[Ppfs-2PFS-2::GFP]*
CZ9399	*juEx1939[Ppfs-2PFS-2::GFP]*
Synaptic marker strains	
CZ4574	*sydn-1(ju541);juIs1*
CZ4559	*sydn-1(ju541);rpm-1(ju44);juIs1*
CZ455	*rpm-1(ju44);juIs1*
CZ8227	*sydn-1(ju541);nuIs152*
KP3292	*nuIs152*
CZ4739	*sydn-1(ju541);syd-2(ju37);juIs1*
CZ4926	*syd-2(ju37);juIs1*
CZ4766	*sydn-1(ju541);sad-1(ju53);juIs1*
CZ469	*sad-1(ju53);juIs1*
CZ9526	*pfs-2(ju608);juIs1*
CZ9525	*sydn-1(ju541);pfs-2(ju608);juIs1*
Axon marker strains	
CZ4778	*sydn-1(ju541);juIs76*
CZ3432	*syd-2(ju37);juIs76*
CZ3010	*rpm-1(ju44);juIs76*
CZ4784	*sydn-1(ju541);rpm-1(ju44);juIs76*
CZ4767	*sydn-1(ju541);syd-2(ju37);juIs76*
CZ8494	*sydn-1(ju541);syd-1(ju82);juIs76*
CZ5962	*syd-1(ju82);juIs76*
CZ2434	*rpm-1(ju44);syd-2(ju37);juIs76*
CZ8795	*unc-18(e234);juIs76*
CZ8794	*sydn-1(ju541);unc-18(e234);juIs76*
CZ8790	*unc-49(e382);juIs76*
CZ8791	*sydn-1(ju541);unc-49(e382);juIs76*
CZ1915	*unc-119(ju148);juIs76*
CZ8792	*sydn-1(ju541);unc-119(ju148);juIs76*
CZ8828	*sydn-1(ju541);eri-1(mg366);syd-2(ju37);juIs76*
VWL5	*sydn-1(ju541);unc-43(n498); juIs76*
VWL6	*unc-43(n498); juIs76*
VWL7	*sydn-1(ju541);unc-43(n498 n1196); juIs76*
VWL8	*unc-43(n498n1196); juIs76*
CZ8318	*sydn-1(ju541);abi-1(tm494);juIs76*
CZ8316	*abi-1(tm494);juIs76*
CZ8231	*sydn-1(ju541);unc-34(e566);juIs76*
CZ2538	*unc-34(e566);juIs76*

animal (Zhen et al., 2000; Zhen and Jin, 1999; Hallam et al., 2002). Synergistic interactions have been observed among these synapse development mutations. For example, *syd-2;rpm-1* double mutants are severely uncoordinated, with few synapses (Liao et al., 2004; Nakata et al., 2005). Such synergistic interactions indicate that multiple, partly redundant signaling pathways regulate synapse development.

To identify additional pathways in synaptogenesis we mutagenized *rpm-1* animals and searched for double mutants displaying enhanced locomotion defects, which are associated with severe disruptions of synapses, and isolated *sydn-1(ju541)* (see Materials and methods). *sydn-1* single mutants were mildly uncoordinated (Fig. 1A) and exhibited abnormal synapse and axon morphology. We quantified the synaptic defects in *sydn-1* using an SNB-1::GFP marker expressed in GABAergic motoneurons. In wild-type (WT) animals, SNB-1::GFP showed evenly spaced, round, fluorescent puncta in the dorsal and ventral cords. In *sydn-1* mutants, SNB-1::GFP formed fewer puncta and these were abnormally shaped (Fig. 1B). The GFP intensity in the soma was not altered compared with WT, suggesting that *sydn-1* is unlikely to have affected the overall expression levels of the transgene (Fig. 1C). The cholinergic motoneurons revealed similar effects, although these were less severe than for GABAergic neurons (Fig. 1D). Other synapse markers, for the active zone (SYD-2::GFP, SYD-1::GFP) and endosomes (YFP::RAB-5, CFP::RAB-7), were also abnormal (see Fig. S1A in the supplementary material; data not shown). We then verified that these defects were not simply a transgene effect by immunohistochemical staining of two presynaptic proteins. The fluorescence intensities for the synaptic vesicle protein SNT-1 and the active-zone protein ELKS-1 were noticeably reduced in the nerve ring and nerve cords in *sydn-1* mutants, as compared with WT (Fig. 2A,B). The number of ELKS-1-stained puncta in the dorsal nerve cords was significantly reduced in *sydn-1* mutants (Fig. 2C). These analyses reveal that multiple aspects of *sydn-1* mutant synapses are abnormal.

We also examined axon morphology in the *sydn-1* mutants. Although most axons were grossly normal in their trajectory or axon path, close observation revealed small protrusions (~1-2 μm) from the neuron processes (Fig. 1E,F). For example, in *sydn-1* mutants, 6% of GABAergic motoneurons (n=132 animals) displayed ectopic protrusions compared with none in control animals (n=51) (Fig. 4C). These protrusions extended from variable positions of the dorsal or ventral processes, or commissures. Additionally, in *sydn-1* mutants the GFP-labeled axons often

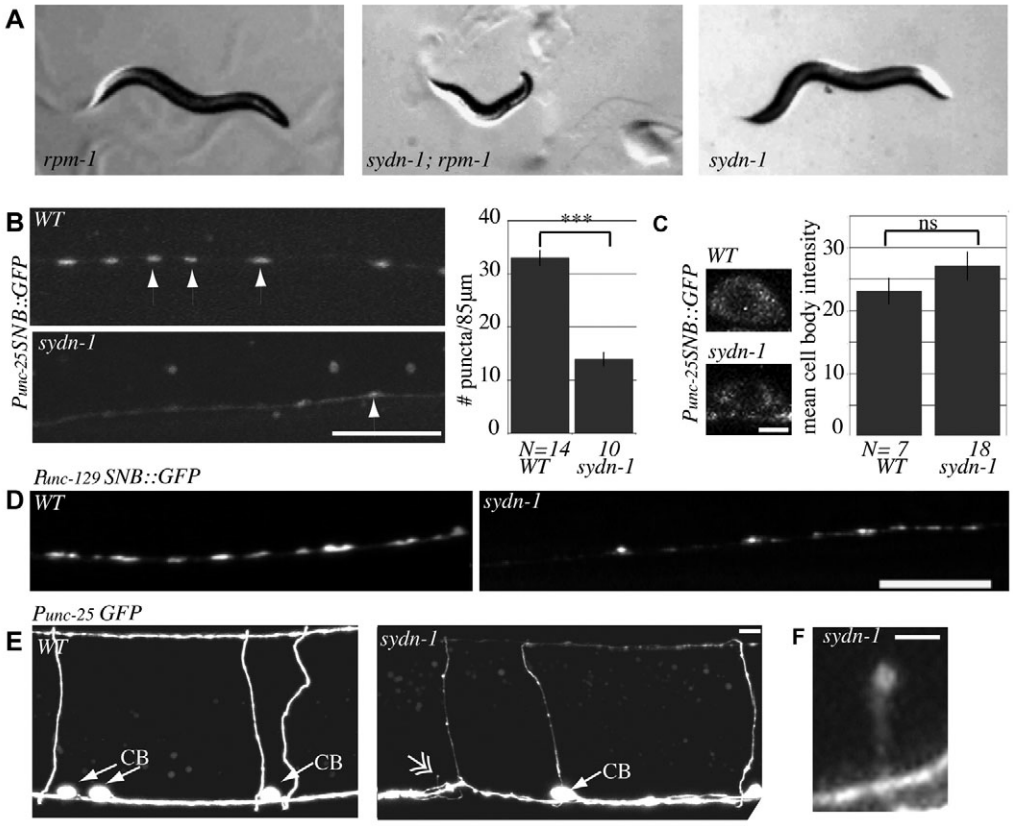

Fig. 1. *C. elegans sydn-1* mutants exhibit abnormal synapses and axons. (**A**) *rpm-1* animals exhibit grossly normal movement. *sydn-1;rpm-1* animals are small and exhibit a severe Unc phenotype. *sydn-1* animals appear normal in size and are mildly Unc. (**B**) SNB-1::GFP in the dorsal nerve cord of GABAergic motoneurons. WT puncta appear round and evenly spaced (arrowheads). In *sydn-1* animals, puncta are unevenly shaped (arrowhead) and fewer in number. Quantification is shown to the right. *N* indicates the number of animals. Error bars indicate s.e.m., here and in all subsequent figures. ***, P<0.001; Student's t-test. (**C**) Soma expression of $P_{unc\text{-}25}$*SNB-1::GFP* in GABAergic motoneurons is unaltered in *sydn-1* animals. Quantification is shown to the right. *N* indicates the number of cell bodies. ns, P>0.3; Student's t-test. (**D**) SNB-1::GFP in the dorsal nerve cord of cholinergic motoneurons. In *sydn-1*, puncta are fewer and unevenly distributed. (**E**) GABAergic neuron morphology is grossly normal in *sydn-1* mutants; however, axonal GFP brightness is noticeably reduced in some regions. The double-headed arrow indicates a small ectopic branch. (**F**) *sydn-1* mutant axons extend ectopic branches. Images in B-F are shown with anterior to the left, ventral down. CB, cell body. Scale bars: 5 μm in B,E; 2 μm in C; 10 μm in D; 1 μm in F.

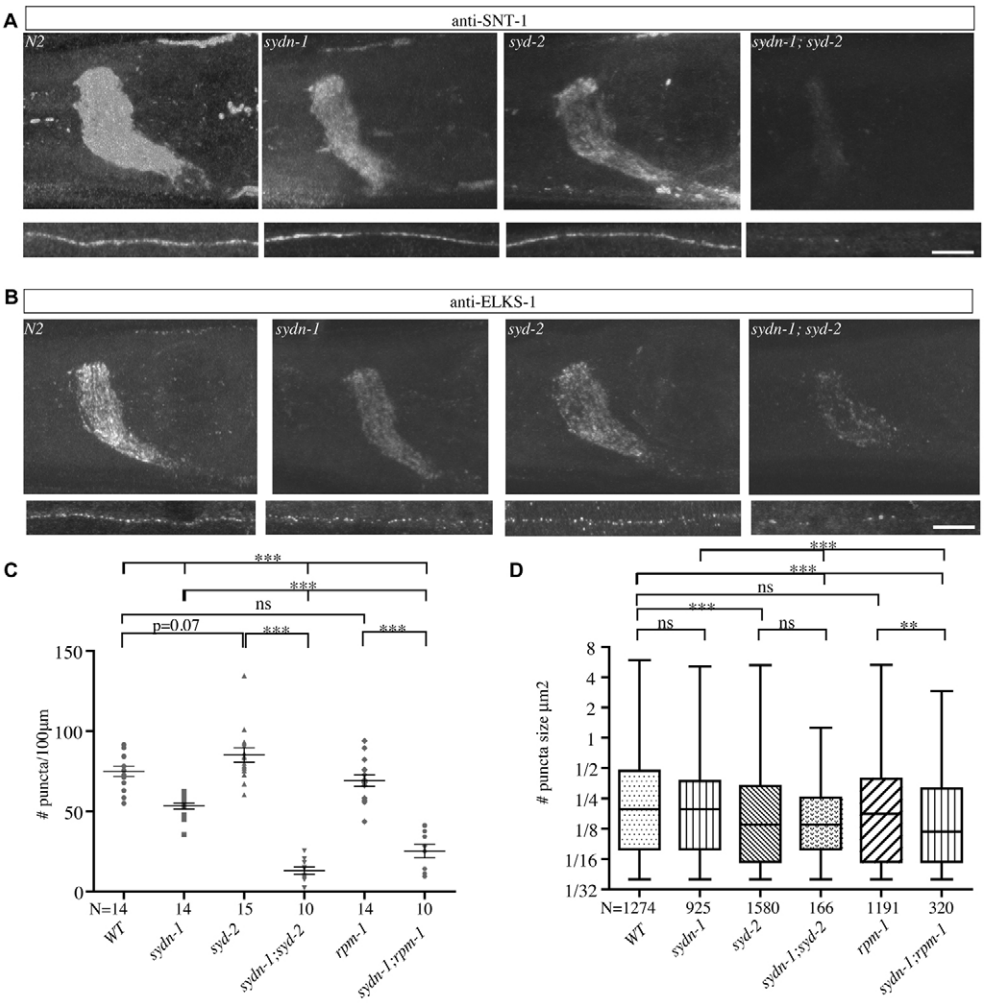

Fig. 2. Endogenous synaptic protein expression is altered in *sydn-1*, *sydn-1;syd-2* and *sydn-1;rpm-1* mutants. (**A**,**B**) Confocal projections of nerve ring (top row) and dorsal nerve cord (bottom row) stained with anti-SNT-1 (A) or anti-ELKS-1 (B). Staining intensity was noticeably decreased in *sydn-1* and was highly exacerbated in *sydn-1;syd-2* double mutants. Scale bars: 100 µm. (**C**) The number of ELKS-1-positive puncta in the dorsal cords. N indicates the number of animals. ns, not significant; ***, $P<0.0001$; Student's *t*-test. (**D**) Quantification of the size of ELKS-1-stained puncta in the dorsal cords. Animals are the same as those in C. N indicates the number of puncta analyzed. Box indicates s.e.m.; the top and bottom lines indicate the minimum and maximum puncta sizes, respectively. ***, $P<0.0001$; **, $P<0.01$; ns, not significant; non-parametric test (GraphPad Prism).

displayed noticeably reduced fluorescence intensity, which was most obvious in the commissures and dorsal processes of the ventral cord neurons, as well as in longitudinal axons of mechanosensory, HSN and PVQ neurons (Fig. 1E; data not shown). The neuronal morphology phenotypes and locomotion deficit of *sydn-1* mutants were visible in young larvae and did not progressively worsen in aged adults, indicating an early defect in development (see Fig. S1B in the supplementary material).

To further evaluate the architecture of the nervous system, we analyzed the ultrastructure of the ventral cord of animals fixed using a high-pressure freeze procedure. The axon membrane bilayer appeared grossly normal in *sydn-1* mutants and the overall left-right asymmetry of the nerve bundle was maintained. Although the left and right bundles still had the same gross number of main axons (Fig. 3A), there were more small axons in *sydn-1* (Fig. 3). Since we did not observe an increase in neuronal number using various GFP reporters (Fig. 1; data not shown), we suspect that the increased number of axon profiles in the *sydn-1* ventral cord is likely to be due to the small axonal protrusions that extend off from the normal axon processes (Fig. 1E).

sydn-1 displays specific synergistic interactions with a set of synapse development genes

To determine whether the behavioral synergy between *sydn-1* and *rpm-1* reflected synergistic effects at the synapse, we examined synaptic morphology in *sydn-1;rpm-1* double mutants. In these animals, the SNB-1::GFP puncta in the GABAergic motoneurons were almost completely absent (Fig. 4A). Immunostaining of ELKS-1 and SNT-1 showed severe reduction in all major areas of the nervous system (Fig. 2C,D; see Fig. S2 in the supplementary material). Such enhanced synaptic defects are consistent with *sydn-1* and *rpm-1* acting in parallel in synapse development.

The altered synapse morphology in *sydn-1* mutants partially resembled the phenotype of the synapse development mutants *syd-1*, *syd-2* and *sad-1* (Crump et al., 2001; Hallam et al., 2002; Zhen and Jin, 1999). We tested genetic interactions of *sydn-1* with these genes. All the double mutants between these three genes and *sydn-1* exhibited enhanced locomotion defects that were independent of transgenes. The synapse morphology showed more severe abnormalities than each single mutant by SNB-1::GFP fluorescence or by immunostaining of SNT-1 and ELKS-1 (Fig. 2, Fig. 4A). More strikingly, we observed an elaboration of axon protrusions in the double mutants (Fig. 4B,C). The aberrant axon morphologies were seen in different types of neurons to varying degrees. For example, both GABAergic and cholinergic motoneurons in *sydn-1;syd-2* animals showed a similar degree of excess axon branching and protrusions, whereas the mechanosensory neurons showed only small axon protrusions (data not shown). These effects on axon morphology were not seen in *rpm-1;syd-2* or *syd-1;syd-2* double mutants (Fig. 4C; data not shown). The observed synergistic interactions indicate that *sydn-1* acts in a novel pathway parallel to those regulated by *rpm-1*, *syd-2*, *syd-1* or *sad-1*.

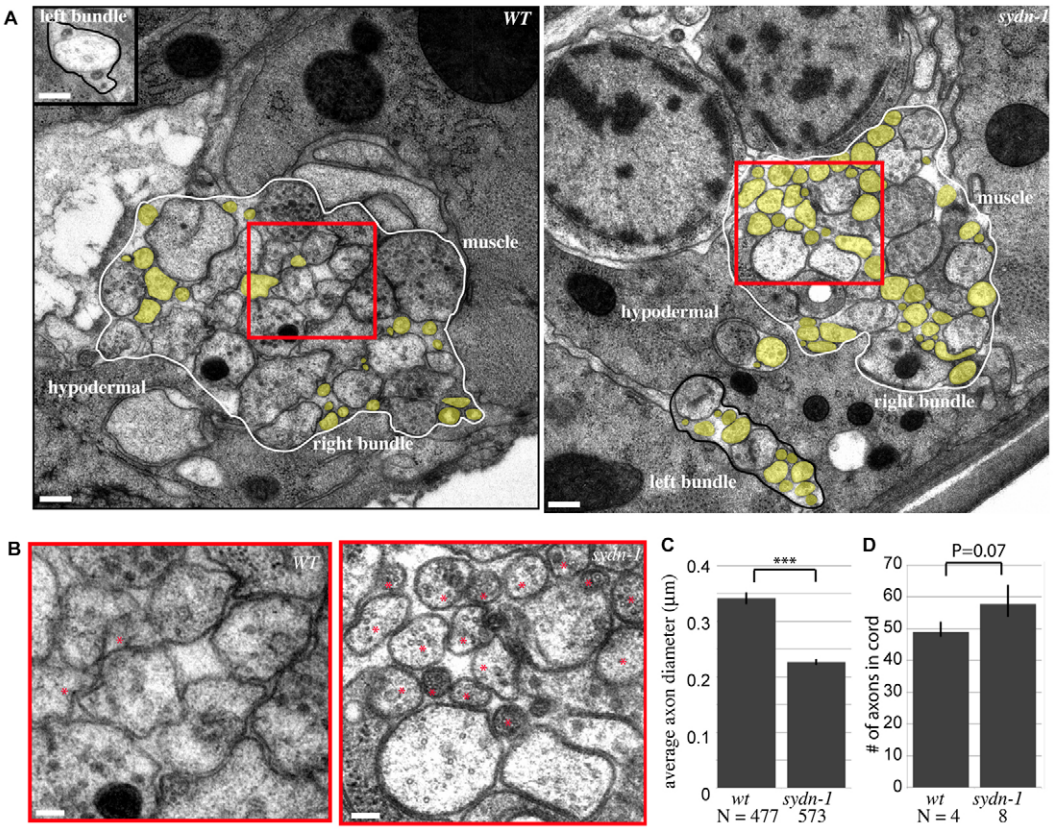

Fig. 3. *sydn-1* mutants show increased numbers of small axonal profiles. (**A**) Electron micrographs of ventral nerve cord cross-sections in WT and *sydn-1* animals. Right bundle is indicated by the white outline, the left bundle by the black outline. Small axons are marked in yellow. (**B**) Magnified view of the red-boxed regions in A. Markedly small axons are marked with an asterisk. (**C**) Reduced axon diameters in *sydn-1* animals. N indicates the number of axons. ***, $P<0.001$; Student's *t*-test. (**D**) Increased number of neurite profiles in *sydn*-1 mutants. N indicates the number of animals. $P=0.07$; Fisher's exact test. Scale bars: 400 nm in A; 200 nm in B.

To further explore the effects of *sydn-1* on synapses, we examined interactions between *sydn-1* and genes that function in synaptic transmission. *unc-18* (mammalian *Munc18*; syntaxin-binding protein) enables synaptic vesicle docking and promotes exocytosis (Weimer et al., 2003). The GABA receptor *unc-49* is required for a postsynaptic GABA response and locomotion (Bamber et al., 1999), but not for morphological development of the synapse (Gally and Bessereau, 2003). *sydn-1;unc-18* and *sydn-1;unc-49* double mutants showed additive deficits in locomotion and did not display strong synergy in axon or synapse morphology phenotypes (Fig. 4C; data not shown). The CaMKII homolog UNC-43 has many roles in the development and function of the synapse (Reiner et al., 1999) and has also been reported to interact with the netrin axon-guidance pathway (Wadsworth, 2002; Wang and Wadsworth, 2002). We analyzed genetic interactions of *sydn-1* with both *unc-43(n498sd)* gain-of-function and *unc-43(n498n1196)* loss-of-function mutants and did not observe strong enhancement of the neuronal or behavioral phenotypes of *sydn-1* mutants (Fig. 4C).

Aberrant axon branching is often associated with cytoskeletal defects. We tested interactions between *sydn-1* and genes that function in axon outgrowth and branching or in cytoskeleton regulation. The Enabled homolog UNC-34 is a regulator of the actin cytoskeleton and is required for axon outgrowth and guidance (Gitai et al., 2003; Withee et al., 2004; Yu et al., 2002). Abelson-interacting protein 1 (ABI-1) interacts with multiple cytoskeleton regulators, including UNC-53, to regulate dendrite outgrowth and morphogenesis (Schmidt et al., 2009). The conserved protein UNC-119 (mammalian Unc119) inhibits axon branching (Knobel et al., 2001). We found that double mutants of *sydn-1(ju541)* with *unc-34*, *abi-1* or *unc-119* displayed overall additive behavioral phenotypes and that the axonal phenotypes were no more severe than for the strongest single mutant (Fig. 4C). In summary, although our genetic double-mutant analysis cannot be exhaustive, these results reveal that *sydn-1* function becomes crucial when synapses are improperly formed.

SYDN-1 is a novel nuclear protein that acts cell-autonomously in neurons

We positionally cloned *sydn-1* and determined that *sydn-1(ju541)* contains a 1 kb deletion in the gene *Y39G10AR.17* (Fig. 5B). Using RACE and RT-PCR we verified the predicted gene structure and obtained full-length *sydn-1* cDNA. SYDN-1 comprises 578 amino acids and has a highly proline-rich C-terminus that contains multiple regions of four to 11 consecutive prolines. Apparent orthologs of SYDN-1 are present in other nematode species. For example, the *C. briggsae* protein (BP:CBP31994) exhibits an overall 58% identity and 71% similarity with SYDN-1.

The 1 kb deletion in *sydn-1(ju541)* removes 193 bp of the promoter and most of the first exon (Fig. 5B). By RT-PCR analysis, we found that the remaining exons 2-5 were transcribed in *sydn-1(ju541)* animals, possibly via a cryptic promoter in the first intron.

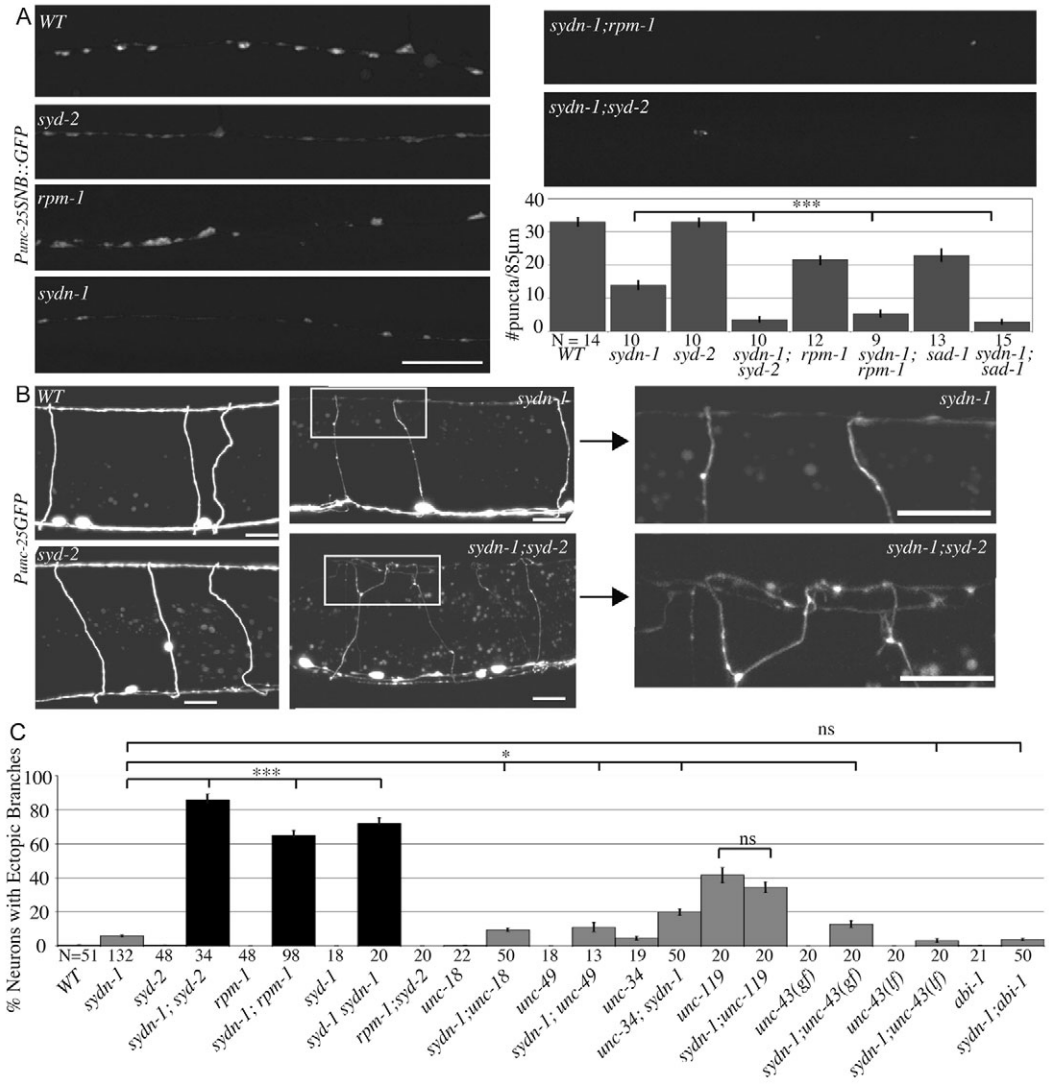

Fig. 4. *sydn-1* synergizes with mutations in synapse development genes. (**A**) SNB-1::GFP in the dorsal cord of GABAergic motoneurons. *syd-2*, *rpm-1* and *sydn-1* exhibit abnormally shaped puncta (left). *sydn-1;syd-2* and *sydn-1;rpm-1* double mutants exhibit reduced numbers of puncta (right, with quantitation in bar chart). N indicates the number of animals. ***, $P<0.001$; Student's *t*-test. (**B**) GFP-labeled GABAergic neuron axons (ventral down and anterior left). *sydn-1;syd-2* double mutants display ectopic and excessive axon branches. A magnified view is shown on the right. (**C**) Quantification of the percentage of neurons per animal that display excess GABAergic neuron axon branches. N indicates the number of animals. *, $P<0.01$; ***, $P<0.001$; ns, $P>0.2$; Student's *t*-test. Scale bars: 5 µm.

Transgenic expression of WT *sydn-1* genomic DNA fully rescued the behavior, axon and synapse defects in *sydn-1(ju541)* (Fig. 5C,D). Overexpression of the mutant genomic region from *sydn-1(ju541)* did not rescue the mutants, nor did it cause any discernable abnormalities in WT. These results show that *ju541* is unlikely to express any active SYDN-1 protein and that the mutant phenotypes are caused by *sydn-1* loss of function.

We determined the *sydn-1* cell-type requirement by tissue-specific expression. Transgenic expression of *sydn-1* from a pan-neuronal promoter (P_{rgef-1}), but not from an epidermal promoter (P_{dpy-7}), fully rescued the locomotion and neuronal phenotypes of *sydn-1* mutants. Expression of the *sydn-1* cDNA under the control of a GABAergic motoneuron promoter (P_{unc-25}) rescued the GABAergic neuron synaptic and axonal morphology phenotypes, but not the locomotion behavior (Fig. 5C,D). These data show that SYDN-1 can act cell-autonomously to promote synaptogenesis and that the movement deficits are likely to result from defects in multiple neuron types.

To determine the subcellular localization of SYDN-1 in neurons, we expressed functional FLAG-tagged SYDN-1 under the control of the *rgef-1* pan-neuronal promoter in *sydn-1* animals (Fig. 5C-F). Immunostaining with anti-FLAG showed that FLAG::SYDN-1 was localized to the nucleus and was frequently enriched where DAPI staining was weak (Fig. 5E, arrows). Within the nucleus, FLAG::SYDN-1 localization appeared either as a speckled pattern or a small subnuclear ring (Fig. 5F) (speckled pattern, 47±5%; ring pattern, 53±5%; average ± s.e.m.; n=1108 nuclei from 39 animals). DAPI staining was frequently observed outside of the subnuclear ring of SYDN-1, suggesting that SYDN-1 is not localized close to the nuclear envelope. Thus, SYDN-1 defines a nuclear component that regulates axon and synapse development.

Loss of function in the 3′-end processing factor PFS-2 suppresses *sydn-1*

To better understand the molecular function of SYDN-1 we conducted a genetic suppressor screen (see Materials and methods). Among the suppressor mutations, we focused on a strong recessive suppressor: allele *ju608*. The abnormal synaptic puncta of *sydn-1(ju541)* animals were completely suppressed by *ju608* (Fig. 6C). Similarly, the increased axon protrusions in *sydn-1;syd-2* animals were completely eliminated by *ju608*, as were the enhanced locomotion defects (Fig. 6D,F). *ju608* single mutants did not display synaptic defects and did not suppress the phenotypes of *syd-2* (Fig. 6C; data not shown). Animals were grossly WT in movement, size and behavior, but showed a significant reduction in brood size (see Fig. S3A in the supplementary material).

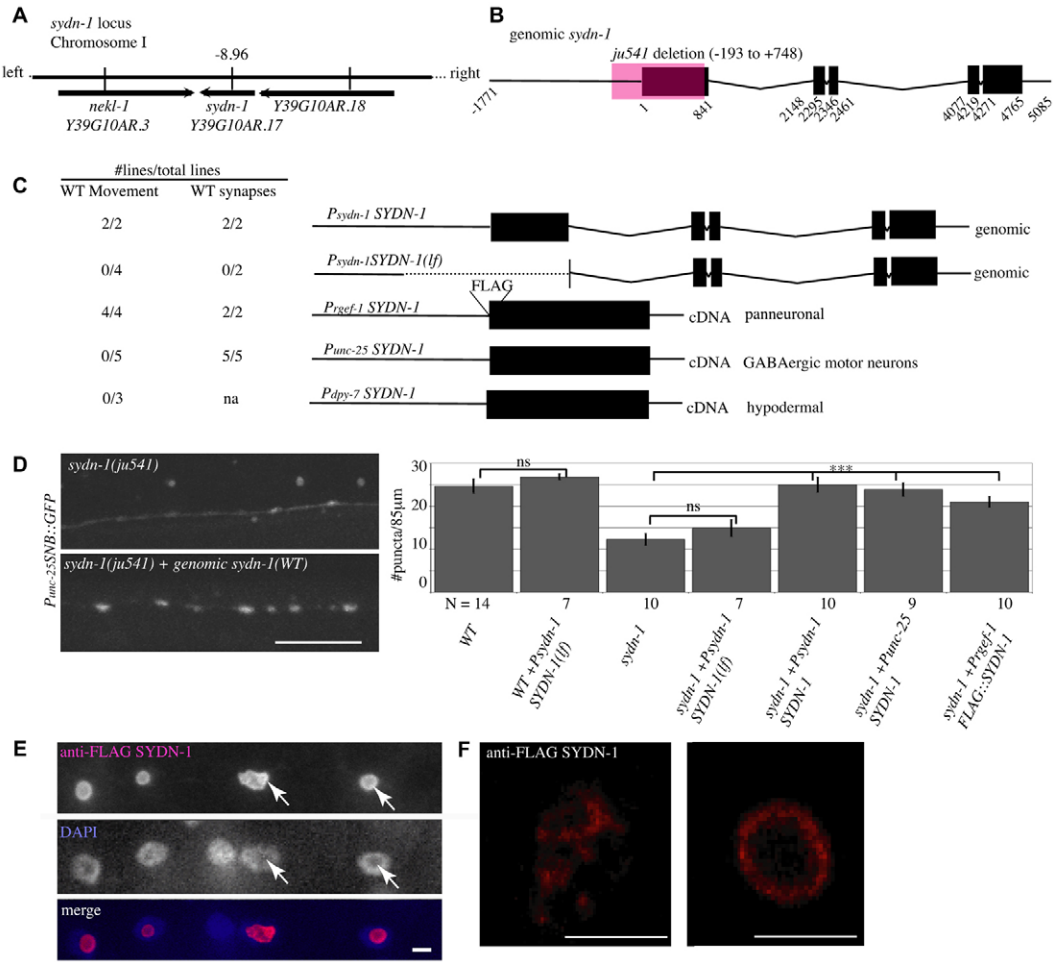

Fig. 5. SYDN-1 is a novel nuclear protein that acts in the nervous system. (**A**) The *C. elegans sydn-1(ju541)* locus is at chromosome I: –8.96. (**B**) The *sydn-1* gene structure. Left straight line, promoter; black boxes, exons; bent lines, introns. *ju541* contains a 1 kb deletion (purple box). (**C**) The *sydn-1* synapse phenotype is rescued by transgenic expression of genomic *sydn-1* (P_{sydn-1}), pan-neuronal-driven *sydn-1* (P_{rgef-1}) and GABAergic neuron-driven *sydn-1* (P_{unc-25}) cDNA. (**D**) Synaptic puncta in transgenically rescued *sydn-1* animals are similar to those of WT (see Fig. 1) in shape, intensity and spacing. Quantitation in the central dorsal cord of transgenically rescued lines is shown to the right. N indicates the number of animals. ***, $P<0.001$; Student's *t*-test. (**E**) Epifluorescence images of the ventral nerve cord of *sydn-1(ju541);Ex*(P_{rgef-1}FLAG::SYDN-1) animals immunostained for FLAG and co-stained with DAPI. Arrows indicate regions of intense SYDN-1 and weak DAPI staining. (**F**) Confocal stacked images of *sydn-1;Ex*(P_{rgef-1}FLAG::SYDN-1) animals stained for FLAG show speckled (left) or ring (right) patterns. Scale bars: 5 µm in D; 2 µm in E,F.

We mapped *ju608* to the right arm of chromosome II, and determined that *ju608* contains a single G-to-A nucleotide transition in the third exon of *pfs-2* (Fig. 6A,B). The suppression activities of *ju608* were fully rescued by transgenic expression of WT *pfs-2* (Fig. 6D-F). PFS-2 is a member of a conserved family of proteins that are characterized by the presence of seven WD repeats at the N-terminus (Fig. 6G), which have been shown to be crucial for yeast Pfs2p function in NpolyA (Ohnacker et al., 2000). The *pfs-2(ju608)* mutation causes an Arg147Gln substitution at a completely conserved residue in the first WD repeat (Fig. 6G). To determine the nature of the *ju608* mutation, we conducted *pfs-2* RNAi using the enhanced RNAi strain *sydn-1;syd-2;eri-1;juIs76*[P_{unc-25}GFP]. *pfs-2* RNAi caused complete sterility (see Fig. S3B in the supplementary material). In order to test the effects of *pfs-2* knockdown in neurons, we treated the animals using a titrated *pfs-2* RNAi approach (see Materials and methods), and observed a complete suppression of the neuronal and behavioral defects in the viable animals (Fig. 6H). Furthermore, overexpression of the full-length *pfs-2(ju608)* mutant genomic DNA in *sydn-1(ju541)* animals did not cause any suppression of the mutant phenotypes (Fig. 6C, bar chart). These data indicate that *pfs-2* is essential for embryo viability and adult fertility and that *ju608* is a recessive partial loss-of-function (plf) mutation.

All Pfs2p homologs in higher eukaryotes have an extended C-terminus that shares little sequence homology among them (Fig. 6G). We tested the role of the C-terminus of PFS-2 by transgenic expression of a truncated genomic DNA containing only the WD-repeat region of PFS-2 and observed that this expression dramatically reduced the rescuing activities in *sydn-1;pfs-2* animals (Fig. 6F). This suggests that the C-terminal extension is required for the function of PFS-2.

SYDN-1 regulates the nuclear abundance of PFS-2

The genetic suppression of *sydn-1(lf)* by *pfs-2(plf)* suggests that PFS-2 might be negatively regulated by SYDN-1. To address the basis of this genetic interaction, we first performed qRT-PCR, and found that SYDN-1 and PFS-2 do not regulate one another's transcript levels (see Fig. S3C in the supplementary material). We

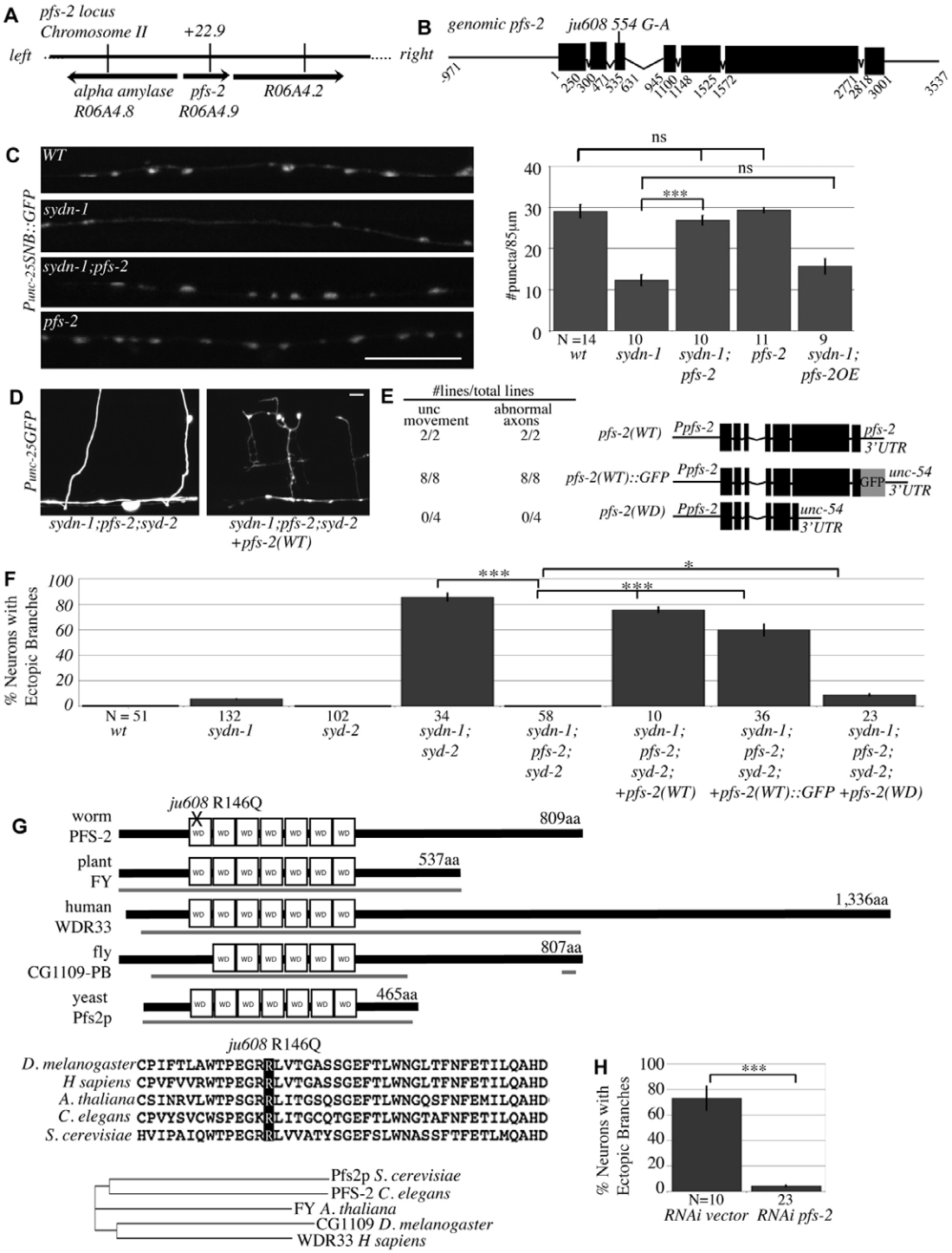

Fig. 6. Loss of function of *pfs-2* suppresses *sydn-1*. (**A**) *C. elegans pfs-2(ju608)* was mapped to chromosome II: +22.9. (**B**) The *pfs-2* gene structure (key as Fig. 5). *ju608* contains a G-to-A nucleotide transition in the third exon, causing an arginine-to-glutamine mutation. (**C**) In *sydn-1;pfs-2*, SNB-1::GFP puncta in the dorsal nerve cord of GABAergic neurons appear normal. Scale bar: 5 µm. Quantification of SNB-1::GFP is shown to the right. Overexpression of *ju608* (*pfs-2OE*) in *sydn-1* does not significantly change the number or characteristics of mutant puncta. N indicates the number of animals. ***, $P<0.0001$; ns, $P>0.3$; Student's *t*-test. (**D**) In *sydn-1;syd-2;pfs-2*, axons are normal in morphology and GFP intensity. Expression of *pfs-2(WT)* rescues the suppression activity of *pfs-2* (right-hand panel). (**E**) Illustrations of transgenic constructs (right) and a summary of transgenic rescue (left). (**F**) Quantitation of *pfs-2(ju608)* suppression activities on ectopic branches. Suppression activity of *pfs-2(ju608)* is not rescued by expression of only the PFS-2 WD-repeat domain. N indicates the number of animals. ***, $P<0.001$; *, $P<0.01$; Student's *t*-test. (**G**) Alignment of PFS-2 with homologs. *S. cerevisiae* Pfs2p, NM_001018284.1; *C. elegans* PFS-2, Z83120.1; *A. thaliana* FY, NM_121351.4; *D. melanogaster* CG1109, NM_169091.1; *H. sapiens* WDR33, NM_018383.3. Gray bar denotes a region that is homologous to *C. elegans* PFS-2 (~57% to ~70% similarity from yeast to human). The *ju608* mutation occurs in a completely conserved arginine in the first WD repeat. A phylogram of PFS-2 homologs is shown at the bottom. (**H**) RNAi knockdown of *pfs-2* suppresses ectopic axon branches in *sydn-1;eri-1;syd-2;*$P_{unc\text{-}25}$*GFP*. N indicates the number of animals. ***, $P<0.001$; Student's *t*-test.

then examined the subcellular localization of both proteins. Expression of a GFP-tagged transgenic PFS-2 ($P_{pfs\text{-}2}$PFS-2::GFP) fully rescued the suppression activity of *pfs-2(ju608)* (Fig. 6E,F), and PFS-2::GFP was localized to nuclei in neuronal and non-neuronal tissues (Fig. 7A). Colocalization studies of neuronally expressed FLAG::SYDN-1 and PFS-2::GFP revealed similar subnuclear patterns, such that within a single nucleus both proteins appeared either as a speckled or a ring pattern (Fig. 7A,B) (n>100 nuclei), with varying degrees of overlap in subnuclear speckles.

We next asked whether the localization of the two proteins depend on each other. FLAG::SYDN-1 nuclear localization was not detectably altered in *pfs-2(ju608)* mutants (Fig. 7C). By contrast, the intensity of PFS-2::GFP was noticeably increased in *sydn-1* mutants compared with WT (Fig. 7C). The frequency of the ring versus speckled pattern of PFS-2::GFP in *sydn-1* was about the same as in WT (for WT, 79±1% speckled and 21±1% ring, n=274 nuclei; for *sydn-1*, 73±1% speckled and 27±1% ring, n=499 nuclei; average ± s.e.m.; P>0.9, Student's t-test).

To test the specificity of the observed effects of *sydn-1(lf)* on PFS-2, we examined the localization of the *C. elegans* ortholog of CstF-64, CPF-2 (Evans et al., 2001). Immunostaining of CPF-2 showed nuclear ring and speckled patterns, and the overall nuclear intensity was comparable in WT and *sydn-1* mutants (see Fig. S4 in the supplementary material). These analyses suggest that SYDN-1 is likely to negatively regulate the activity of PFS-2 by influencing its abundance.

Reducing nuclear polyadenylation activity suppresses *sydn-1* mutant defects

The above observations raise the question of whether suppression of SYDN-1 is mediated by changes in NpolyA activities. We performed RNAi of other NpolyA factors in *sydn-1* mutants. Knockdown of these genes caused lethality and adult sterility in the *sydn-1;syd-2;eri-1;juIs76* strain (data not shown), confirming multiple previously reported RNAi observations (e.g. Kamath et al., 2003; Simmer et al., 2003). We observed partial suppression of the *sydn-1;syd-2;eri-1;juIs76* behavior and axon protrusion phenotypes among the escaper adult progeny from animals treated with RNAi targeting the 3′-end processing factors *cpf-1*, *cpf-2*, *cpsf-2*, *cids-1* and *cids-2*, and a putative PAP, *t15h9.6* (Fig. 8A). By contrast, RNAi knockdown of three other PAPs (*F43G6.5*, *pap*-1, *gld-2*) did not show significant effects on Sydn-1 defects, consistent with studies implicating these genes in other types of RNA regulation (Cui et al., 2008; de la Mata and Kornblihtt, 2006; Maciolek and McNally, 2007; Meinhart and Cramer, 2004; Wang et al., 2002). These observations show that aberrant synaptic and axonal development in *sydn-1* mutants can be ameliorated by specific reduction of nuclear pre-mRNA 3′-end processing activities.

sydn-1 and *pfs-2* regulate nuclear 3′-end processing activities

To further address whether *pfs-2* and *sydn-1* themselves directly function in NpolyA, we tested their genetic interactions with *lin-15(n765ts)*, the mutant phenotype of which can be modulated by NpolyA activities. *lin-15* encodes an operon of two transcripts, *lin-15A* and *lin-15B*, and controls vulva formation (Clark et al., 1994; Ferguson et al., 1987; Huang et al., 1994). The *lin-15(n765ts)* allele exhibits a temperature-sensitive multivulval phenotype (Muv) owing to the insertion of an NpolyA signal from the gene *H18N23.2* into *lin-15B* (Fig. 8B) (Cui et al., 2008). The insertion disrupts the *lin-15B* transcript, but also causes a reduction of the downstream *lin-15A* transcript owing to abnormal NpolyA and transcriptional termination. Inhibiting NpolyA activities can suppress the Muv defect of *lin-15(n765ts)* (Cui et al., 2008). We found that *pfs-2(ju608)* almost completely suppressed the Muv phenotype of *lin-15(n765ts)* (Fig. 8C,E). Conversely, *sydn-1(ju541)* enhanced the number of multivulval protrusions (Fig. 8D,E).

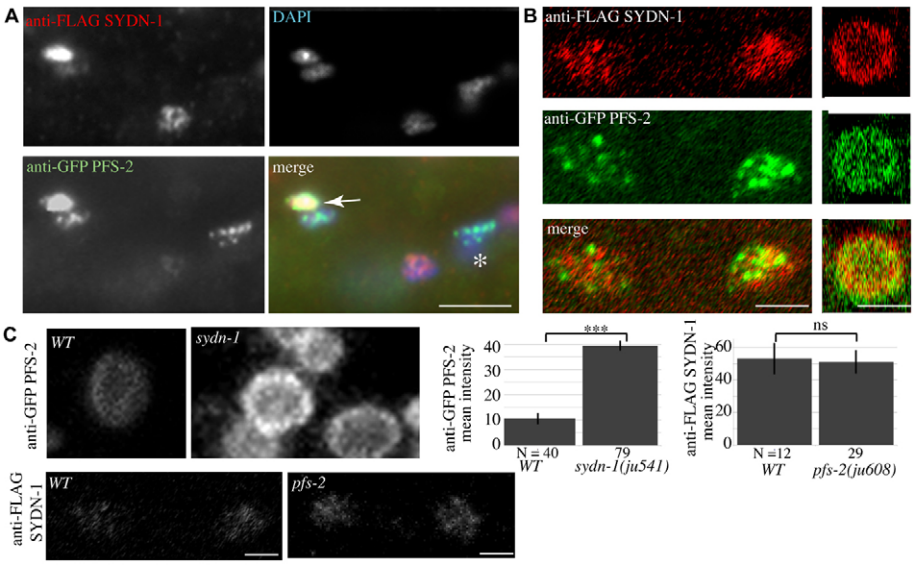

Fig. 7. SYDN-1 regulates PFS-2 abundance. (**A**) Single-plane confocal images of the head region of WT animals expressing a $P_{pfs\text{-}2}$ PFS-2::GFP; $P_{rgef\text{-}1}$ FLAG::SYDN-1 transgene, immunostained for anti-GFP, anti-FLAG and stained for DAPI. PFS-2 and SYDN-1 are colocalized to the nucleus in neurons (arrow). PFS-2 is seen in non-neuronal nuclei (asterisk) due to expression from its endogenous promoter. (**B**) Confocal single-plane images of WT animals expressing a $P_{pfs\text{-}2}$ PFS-2::GFP; $P_{rgef\text{-}1}$ FLAG::SYDN-1 transgene show partial colocalization between PFS-2::GFP and FLAG::SYDN-1. PFS-2 and SYDN-1 together appear speckled (left) or as a smooth ring (right). (**C**) Confocal images of $P_{pfs\text{-}2}$ PFS-2::GFP immunostained with anti-GFP in WT or *sydn-1* (top). P_{rgef}-FLAG::SYDN-1 immunostained with anti-FLAG is not changed in *pfs-2* mutants (below). Quantitation of fluorescence intensity is shown on the right. N indicates the number of nuclei. ***, P<0.001; ns, P>0.5; Student's t-test. Scale bars: 5 μm in A; 2 μm in B,C.

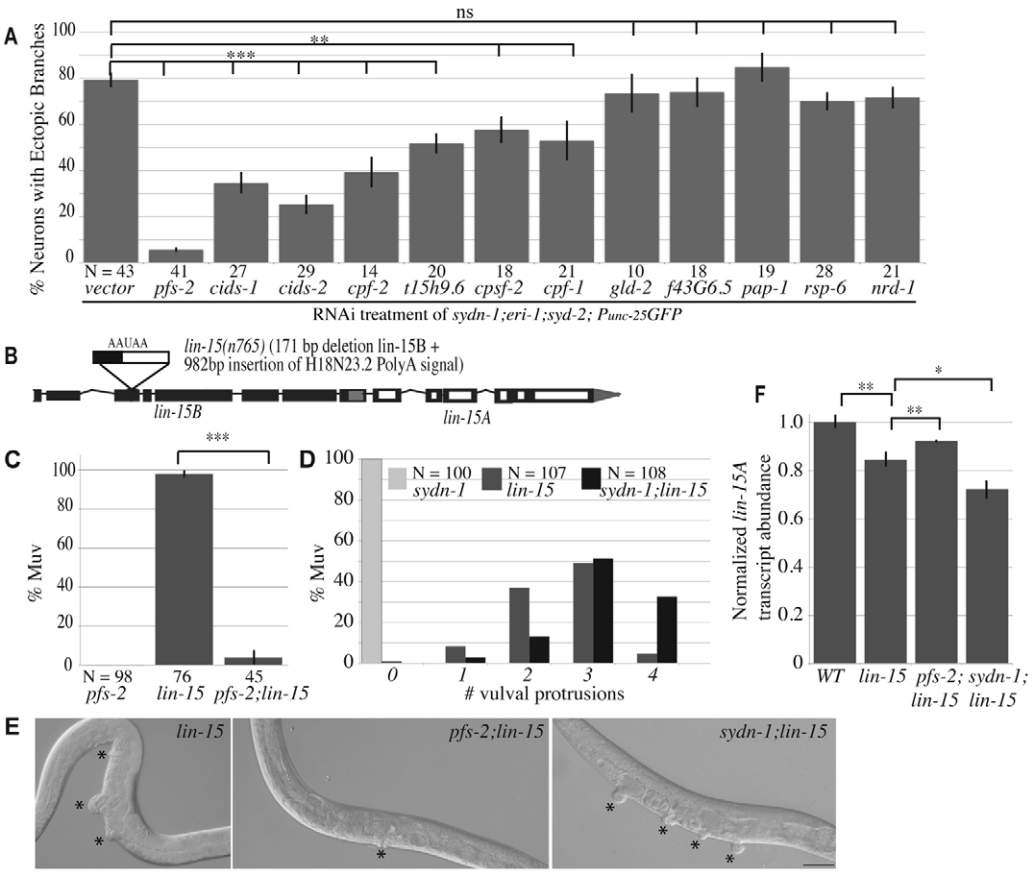

Fig. 8. NpolyA activities are elevated in *sydn-1* mutants. (**A**) RNAi knockdown of several polyadenylation components suppresses ectopic branching in *sydn-1;eri-1;syd-2;*$P_{unc\text{-}25}$*GFP* animals. The percentage of ectopic branches is the percentage of neurons per animal that display excess axon protrusions. Vector control is the L4440 RNAi vector. N indicates the number of animals. ***, P<0.0001; **, P<0.001; ns, P>0.07; Student's t-test. (**B**) The NpolyA site insertion in *lin-15B* in *lin-15(n765ts)* animals (Cui et al., 2008). (**C**) *pfs-2* suppresses the Muv phenotype of *lin-15(n765ts)* animals. N indicates the number of animals. ***, P<0.001; Student's t-test. (**D**) *sydn-1;lin-15(n765ts)* animals display statistically increased numbers of vulval protrusions. N indicates the number of animals. Average number of vulval protrusions: *lin-15(n765)*, 2.5±0.07; *sydn-1(ju541);lin-15(n765)*, 3.1±0.07; average ± s.e.m.; P<0.00001, Student's t-test. (**E**) Examples of Muv phenotypes. Vulval protrusions (asterisk). Scale bar: 50 μm. (**F**) qRT-PCR of *lin-15A* transcript levels normalized to *ama-1* transcript levels and displayed relative to WT. **, P<0.01; *, P<0.05; Student's t-test.

To address whether these genetic interactions reflected molecular changes in NpolyA activity, we performed qRT-PCR on *lin-15A* transcripts. The levels of *lin-15A* transcript were decreased in *lin-15(n765ts)* compared with WT (Fig. 8F), as reported previously (Cui et al., 2008). The levels of *lin-15A* transcripts were increased in *pfs-2(ju608);lin-15(n765ts)* animals, and were decreased in *sydn-1;lin-15(n765ts)* animals, compared with *lin-15(n765ts)* (Fig. 8F). Although a role of *lin-15* in neuronal tissues has been inferred (Kennedy et al., 2004), our findings of *sydn-1* and *pfs-2* effects on *lin-15* pre-mRNA processing are likely to include changes in non-neuronal tissues. Nonetheless, these observations lend support to the proposal that *pfs-2* and *sydn-1* function in NpolyA and imply that elevation or misregulation of NpolyA activities underlies the neuronal phenotypes in *sydn-1* mutants.

DISCUSSION

Using modifier genetics, we have uncovered two proteins that together regulate NpolyA activities in neuronal development. Our data show that NpolyA becomes crucial when synapses are improperly formed and that the novel protein SYDN-1 negatively controls NpolyA activities, in part through influencing the nuclear abundance of PFS-2.

SYDN-1 is a novel regulator of neuronal development

sydn-1(lf) mutants display synaptic abnormalities and uncoordinated locomotion. The uncoordinated phenotype is due to neuronal defects because Sydn-1 phenotypes are fully rescued by cell-specific SYDN-1 expression in the nervous system. The movement defect is likely to reflect a developmental role of *sydn-1* in neurons. First, synapses in *sydn-1* mutants are fewer in number and those that remain often have abnormal morphology. Second, the axons of *sydn-1* mutants frequently exhibit ectopic protrusions and appear to be thin in diameter. Third, the phenotypes of *sydn-1* single mutants are early onset and do not progressively worsen with age. Last, synthetic defects are seen when *sydn-1* is placed in combination with other synapse development mutations, but not with mutations affecting synapse transmission or general axon growth. The combination of phenotypes observed in *sydn-1* mutants has not been seen in the numerous reported *C. elegans* synapse mutants. Our genetic double-mutant analysis, although not exhaustive, indicates that *sydn-1* is a member of a novel pathway acting in parallel to known synapse development pathways and that the activity of *sydn-1* is particularly sensitized to disruptions in synapse

architecture. The enhanced defects in axon morphology of double mutants between *sydn-1* and synaptic architecture genes further suggest a coordination in cellular differentiation between synapse assembly and axonal morphogenesis.

SYDN-1 negatively regulates nuclear pre-mRNA 3′-end processing

Via a second forward genetic screen, we found that the mutant phenotypes of *sydn-1* are strongly suppressed by reduction of function in PFS-2, a member of a conserved protein family implicated in the stabilization of the nuclear 3′-end processing complex (Ohnacker et al., 2000; Shi et al., 2009; Simpson et al., 2003; Wang et al., 2005). Knockdown of several conserved NpolyA components suppresses the *sydn-1* mutant phenotypes to varying degrees, resembling the effects of *pfs-2(plf)*. The Muv suppression of *lin-15(n765ts)* and the increase in *lin-15A* transcripts by *pfs-2(plf)* are consistent with a role of PFS-2 in promoting NpolyA (Cui et al., 2008) (this study). Conversely, the Muv enhancement and the decrease in *lin-15A* transcripts by *sydn-1(lf)* are consistent with SYDN-1 inhibition of NpolyA. We surveyed a set of neuronal genes, including *syd-2*, *snt-1*, *rpm-1* and *unc-43*, and did not detect any significant changes in their overall transcript levels in *sydn-1* and *pfs-2* mutants (data not shown). As these genes do not undergo alternative 3′-end processing, these preliminary observations are consistent with a hypothesis that the interaction between *sydn-1* and *pfs-2* is unlikely to result in a general effect on the stability of all neuronal transcripts, but rather plays specific roles in the control of alternative 3′-end processing, leading to transcripts that play more regulatory roles in response to synapse development signals. The genetic synergistic interactions between *sydn-1* and the other synaptogenesis mutants suggest that this regulation of pre-mRNA processing is particularly crucial when synapses are improperly formed.

Subnuclear compartmentalization in neurons

Both SYDN-1 and PFS-2 display ring-shaped and speckled subnuclear localization patterns. In the absence of SYDN-1, PFS-2 appears more abundant, particularly in the ring-shaped conformation. We do not know the nature or significance of these distinct subnuclear conformations, nor whether the nuclei dynamically convert from one conformation to the other, or, simply, that the ring-shaped pattern is more visible and hence changes are more apparent.

An increasing number of studies have shown that dynamic and distinct nuclear compartments are likely to be associated with various pre-mRNA processing activities in many cell types (Boronenkov et al., 1998; Cardinale et al., 2007; Huang and Spector, 1991; Huang and Spector, 1992; Lamond and Spector, 2003; Mellman et al., 2008; Mintz and Spector, 2000; Politz et al., 2006). SYDN-1 could negatively regulate NpolyA activity on selected transcripts via direct interaction with PFS-2, or indirectly via additional proteins. PFS2 proteins are defined by highly conserved WD repeats, with a divergent C-terminus that is present only in higher eukaryotes. In our RNAi studies of other NpolyA proteins, none was as strong as *pfs-2* in suppressing *sydn-1*. Conceivably, the WD-repeat domain is required for constitutive NpolyA activities and the C-terminal extension of PFS-2 possibly allows binding of additional regulatory factors in a tissue- or context-specific manner. The observation that transgenic expression of PFS-2 lacking the C-terminal extension does not rescue the suppression activities of PFS-2 is consistent with this idea.

Recent studies in *C. elegans* have identified multiple nuclear RNA-binding proteins that localize to subnuclear speckles in neurons, including the CELF/BrunoL ortholog UNC-75, the ELAV-like protein EXC-7, and the putative RNA-binding protein SYD-9 (Loria et al., 2003; Wang et al., 2006). Interestingly, these RNA-binding proteins show specific synergistic genetic interactions with mutations that affect synaptic transmission but not synaptic development. Such distinct genetic synergy implies that these proteins, which include SYDN-1 and PFS-2, are likely to regulate unique pools of RNA targets involved in neuronal development or function, and suggests that complex parallel signaling pathways operate at the level of pre-mRNAs.

Pre-mRNA 3′-end processing as a regulatory pathway in the nervous system

A recent series of reports suggest that alternative pre-mRNA 3′-end processing is an important regulatory process (Lutz, 2008). Specific tissues, including those within the immune system and brain, appear to have a high tendency for biased use of polyadenylation signals (Wang et al., 2008; Zhang et al., 2005). This might be due to the tissue-specific expression of genes that encode pre-mRNA 3′-end processing machinery or differences in the sensitivity of NpolyA cis-regulatory elements (Hunt, 2008). Levels of 3′-end processing factors, such as CstF-64, can influence the production of isoform-specific mRNA for immunoglobulin genes (Takagaki and Manley, 1998). Competition between the RNA-binding protein Sex lethal and CstF-64 also results in the production of different sex-specific isoforms of the same gene through alternative polyadenylation in the *Drosophila* germline (Gawande et al., 2006). In *C. elegans* the CstF-64 homolog CPF-2 has been shown to be preferentially associated with SL2-containing small nuclear ribonucleoproteins (SnRNPs), possibly exerting regulation on transcripts within operons (Evans et al., 2001). We propose that the regulation of PFS-2 and NpolyA by SYDN-1 is likely to confer regulated NpolyA activity on selected neuronal transcripts, either via use of alternative pre-mRNA 3′-end processing sites or tissue-specific NpolyA complexes. A cohort of coordinately regulated transcripts could contribute to the temporal and spatial regulation of synapse and axon development.

Acknowledgements

We thank Min Han and Mingxue Cui for the *lin-15(n765ts)* strain; Mike Nonet and Tom Blumenthal for antibodies; Peg Scott and Tiep Ly for strain construction and maintenance; Benjamin Rollins, Julia Cochran and P. Clint Spiegel for technical assistance; Andrew Chisholm and Mark Palfreyman for comments on the manuscript; and members of our laboratory for discussion. Some strains were obtained from the *Caenorhabditis* Genetics Center, which is supported by grants from the National Institute of Health. This work was supported by a UCOP President's Postdoctoral Fellowship to H.V.E. and an NIH grant (R01 35546) to Y.J. Y.D. and A.G. are Research Associates of, and Y.J. is an investigator of, the Howard Hughes Medical Institute. Deposited in PMC for release after 6 months.

Competing interests statement

The authors declare no competing financial interests.

Supplementary material

Supplementary material for this article is available at
http://dev.biologists.org/lookup/suppl/doi:10.1242/dev.049692/-/DC1

References

Bamber, B. A., Beg, A. A., Twyman, R. E. and Jorgensen, E. M. (1999). The Caenorhabditis elegans unc-49 locus encodes multiple subunits of a heteromultimeric GABA receptor. *J. Neurosci.* **19**, 5348-5359.

Bloch, J. C., Perrin, F. and Lacroute, F. (1978). Yeast temperature-sensitive mutants specifically impaired in processing of poly(A)-containing RNAs. *Mol. Gen. Genet.* **165**, 123-127.

Boronenkov, I. V., Loijens, J. C., Umeda, M. and Anderson, R. A. (1998). Phosphoinositide signaling pathways in nuclei are associated with nuclear speckles containing pre-mRNA processing factors. *Mol. Biol. Cell* **9**, 3547-3560.
Brenner, S. (1974). The genetics of Caenorhabditis elegans. *Genetics* **77**, 71-94.
Cardinale, S., Cisterna, B., Bonetti, P., Aringhieri, C., Biggiogera, M. and Barabino, S. M. (2007). Subnuclear localization and dynamics of the Pre-mRNA 3′ end processing factor mammalian cleavage factor I 68-kDa subunit. *Mol. Biol. Cell* **18**, 1282-1292.
Clark, S. G., Lu, X. and Horvitz, H. R. (1994). The Caenorhabditis elegans locus lin-15, a negative regulator of a tyrosine kinase signaling pathway, encodes two different proteins. *Genetics* **137**, 987-997.
Crump, J. G., Zhen, M., Jin, Y. and Bargmann, C. I. (2001). The SAD-1 kinase regulates presynaptic vesicle clustering and axon termination. *Neuron* **29**, 115-129.
Cui, M., Allen, M. A., Larsen, A., Macmorris, M., Han, M. and Blumenthal, T. (2008). Genes involved in pre-mRNA 3′-end formation and transcription termination revealed by a lin-15 operon Muv suppressor screen. *Proc. Natl. Acad. Sci. USA* **105**, 16665-16670.
Danckwardt, S., Hentze, M. W. and Kulozik, A. E. (2008). 3′ end mRNA processing: molecular mechanisms and implications for health and disease. *EMBO J.* **27**, 482-498.
de la Mata, M. and Kornblihtt, A. R. (2006). RNA polymerase II C-terminal domain mediates regulation of alternative splicing by SRp20. *Nat. Struct. Mol. Biol.* **13**, 973-980.
Deken, S. L., Vincent, R., Hadwiger, G., Liu, Q., Wang, Z. W. and Nonet, M. L. (2005). Redundant localization mechanisms of RIM and ELKS in *Caenorhabditis elegans*. *J. Neurosci.* **25**, 5975-5983.
Evans, D., Perez, I., MacMorris, M., Leake, D., Wilusz, C. J. and Blumenthal, T. (2001). A complex containing CstF-64 and the SL2 snRNP connects mRNA 3′ end formation and trans-splicing in C. elegans operons. *Genes Dev.* **15**, 2562-2571.
Ferguson, E. L., Sternberg, P. W. and Horvitz, H. R. (1987). A genetic pathway for the specification of the vulval cell lineages of Caenorhabditis elegans. *Nature* **326**, 259-267.
Finney, M. and Ruvkun, G. (1990). The unc-86 gene product couples cell lineage and cell identity in C. elegans. *Cell* **63**, 895-905.
Flavell, S. W., Kim, T. K., Gray, J. M., Harmin, D. A., Hemberg, M., Hong, E. J., Markenscoff-Papadimitriou, E., Bear, D. M. and Greenberg, M. E. (2008). Genome-wide analysis of MEF2 transcriptional program reveals synaptic target genes and neuronal activity-dependent polyadenylation site selection. *Neuron* **60**, 1022-1038.
Fraser, A. G., Kamath, R. S., Zipperlen, P., Martinez-Campos, M., Sohrmann, M. and Ahringer, J. (2000). Functional genomic analysis of C. elegans chromosome I by systematic RNA interference. *Nature* **408**, 325-330.
Gally, C. and Bessereau, J. L. (2003). GABA is dispensable for the formation of junctional GABA receptor clusters in Caenorhabditis elegans. *J. Neurosci.* **23**, 2591-2599.
Gawande, B., Robida, M. D., Rahn, A. and Singh, R. (2006). Drosophila Sex-lethal protein mediates polyadenylation switching in the female germline. *EMBO J.* **25**, 1263-1272.
Gitai, Z., Yu, T. W., Lundquist, E. A., Tessier-Lavigne, M. and Bargmann, C. I. (2003). The netrin receptor UNC-40/DCC stimulates axon attraction and outgrowth through enabled and, in parallel, Rac and UNC-115/AbLIM. *Neuron* **37**, 53-65.
Hallam, S. J., Goncharov, A., McEwen, J., Baran, R. and Jin, Y. (2002). SYD-1, a presynaptic protein with PDZ, C2 and rhoGAP-like domains, specifies axon identity in C. elegans. *Nat. Neurosci.* **5**, 1137-1146.
Huang, L. S., Tzou, P. and Sternberg, P. W. (1994). The lin-15 locus encodes two negative regulators of Caenorhabditis elegans vulval development. *Mol. Biol. Cell* **5**, 395-411.
Huang, S. and Spector, D. L. (1991). Nascent pre-mRNA transcripts are associated with nuclear regions enriched in splicing factors. *Genes Dev.* **5**, 2288-2302.
Huang, S. and Spector, D. L. (1992). U1 and U2 small nuclear RNAs are present in nuclear speckles. *Proc. Natl. Acad. Sci. USA* **89**, 305-308.
Hunt, A. G. (2008). Messenger RNA 3′ end formation in plants. *Curr. Top. Microbiol. Immunol.* **326**, 151-177.
Kamath, R. S., Martinez-Campos, M., Zipperlen, P., Fraser, A. G. and Ahringer, J. (2001). Effectiveness of specific RNA-mediated interference through ingested double-stranded RNA in Caenorhabditis elegans. *Genome Biol.* **2**, RESEARCH0002.
Kamath, R. S., Fraser, A. G., Dong, Y., Poulin, G., Durbin, R., Gotta, M., Kanapin, A., Le Bot, N., Moreno, S., Sohrmann, M. et al. (2003). Systematic functional analysis of the *Caenorhabditis elegans* genome using RNAi. *Nature* **421**, 231-237.
Kennedy, S., Wang, D. and Ruvkun, G. (2004). A conserved siRNA-degrading RNase negatively regulates RNA interference in C. elegans. *Nature* **427**, 645-649.
Knobel, K. M., Davis, W. S., Jorgensen, E. M. and Bastiani, M. J. (2001). UNC-119 suppresses axon branching in C. elegans. *Development* **128**, 4079-4092.
Lamond, A. I. and Spector, D. L. (2003). Nuclear speckles: a model for nuclear organelles. *Nat. Rev. Mol. Cell Biol.* **4**, 605-612.
Liao, E. H., Hung, W., Abrams, B. and Zhen, M. (2004). An SCF-like ubiquitin ligase complex that controls presynaptic differentiation. *Nature* **430**, 345-350.
Licatalosi, D. D., Mele, A., Fak, J. J., Ule, J., Kayikci, M., Chi, S. W., Clark, T. A., Schweitzer, A. C., Blume, J. E., Wang, X. et al. (2008). HITS-CLIP yields genome-wide insights into brain alternative RNA processing. *Nature* **456**, 464-469.
Loria, P. M., Duke, A., Rand, J. B. and Hobert, O. (2003). Two neuronal, nuclear-localized RNA binding proteins involved in synaptic transmission. *Curr. Biol.* **13**, 1317-1323.
Lutz, C. S. (2008). Alternative polyadenylation: a twist on mRNA 3′ end formation. *ACS Chem. Biol.* **3**, 609-617.
Maciolek, N. L. and McNally, M. T. (2007). Serine/arginine-rich proteins contribute to negative regulator of splicing element-stimulated polyadenylation in rous sarcoma virus. *J. Virol.* **81**, 11208-11217.
Maftahi, M., Gaillardin, C. and Nicaud, J. M. (1998). Generation of Saccharomyces cerevisiae deletants and basic phenotypic analysis of eight novel genes from the left arm of chromosome XIV. *Yeast* **14**, 271-280.
Mandel, C. R., Bai, Y. and Tong, L. (2008). Protein factors in pre-mRNA 3′-end processing. *Cell. Mol. Life Sci.* **65**, 1099-1122.
Mayr, C. and Bartel, D. P. (2009). Widespread shortening of 3′UTRs by alternative cleavage and polyadenylation activates oncogenes in cancer cells. *Cell* **138**, 673-684.
Meinhart, A. and Cramer, P. (2004). Recognition of RNA polymerase II carboxy-terminal domain by 3′-RNA-processing factors. *Nature* **430**, 223-226.
Mellman, D. L., Gonzales, M. L., Song, C., Barlow, C. A., Wang, P., Kendziorski, C. and Anderson, R. A. (2008). A PtdIns4,5P2-regulated nuclear poly(A) polymerase controls expression of select mRNAs. *Nature* **451**, 1013-1017.
Mello, C. C., Kramer, J. M., Stinchcomb, D. and Ambros, V. (1991). Efficient gene transfer in C. elegans: extrachromosomal maintenance and integration of transforming sequences. *EMBO J.* **10**, 3959-3970.
Mintz, P. J. and Spector, D. L. (2000). Compartmentalization of RNA processing factors within nuclear speckles. *J. Struct. Biol.* **129**, 241-251.
Moore, M. J. and Proudfoot, N. J. (2009). Pre-mRNA processing reaches back to transcription and ahead to translation. *Cell* **136**, 688-700.
Nakata, K., Abrams, B., Grill, B., Goncharov, A., Huang, X., Chisholm, A. D. and Jin, Y. (2005). Regulation of a DLK-1 and p38 MAP kinase pathway by the ubiquitin ligase RPM-1 is required for presynaptic development. *Cell* **120**, 407-420.
Niibori, Y., Hayashi, F., Hirai, K., Matsui, M. and Inokuchi, K. (2007). Alternative poly(A) site-selection regulates the production of alternatively spliced vesl-1/homer1 isoforms that encode postsynaptic scaffolding proteins. *Neurosci. Res.* **57**, 399-410.
Nonet, M. L., Grundahl, K., Meyer, B. J. and Rand, J. B. (1993). Synaptic function is impaired but not eliminated in *C. elegans* mutants lacking synaptotagmin. *Cell* **73**, 1291-1305.
Ohnacker, M., Barabino, S. M., Preker, P. J. and Keller, W. (2000). The WD-repeat protein pfs2p bridges two essential factors within the yeast pre-mRNA 3′-end-processing complex. *EMBO J.* **19**, 37-47.
Politz, J. C., Tuft, R. A., Prasanth, K. V., Baudendistel, N., Fogarty, K. E., Lifshitz, L. M., Langowski, J., Spector, D. L. and Pederson, T. (2006). Rapid, diffusional shuttling of poly(A) RNA between nuclear speckles and the nucleoplasm. *Mol. Biol. Cell* **17**, 1239-1249.
Preker, P. J., Ohnacker, M., Minvielle-Sebastia, L. and Keller, W. (1997). A multisubunit 3′ end processing factor from yeast containing poly(A) polymerase and homologues of the subunits of mammalian cleavage and polyadenylation specificity factor. *EMBO J.* **16**, 4727-4737.
Reiner, D. J., Newton, E. M., Tian, H. and Thomas, J. H. (1999). Diverse behavioural defects caused by mutations in Caenorhabditis elegans unc-43 CaM kinase II. *Nature* **402**, 199-203.
Schmidt, K. L., Marcus-Gueret, N., Adeleye, A., Webber, J., Baillie, D. and Stringham, E. G. (2009). The cell migration molecule UNC-53/NAV2 is linked to the ARP2/3 complex by ABI-1. *Development* **136**, 563-574.
Shi, Y., Di Giammartino, D. C., Taylor, D., Sarkeshik, A., Rice, W. J., Yates, J. R., 3rd, Frank, J. and Manley, J. L. (2009). Molecular architecture of the human pre-mRNA 3′ processing complex. *Mol. Cell* **33**, 365-376.
Simmer, F., Moorman, C., van der Linden, A. M., Kuijk, E., van den Berghe, P. V., Kamath, R. S., Fraser, A. G., Ahringer, J. and Plasterk, R. H. A. (2003). Genome-wide RNAi of *C. elegans* using the hypersensitive rrf-3 strain reveals novel gene functions. *PLoS Biol.* **1**, E12.
Simpson, G. G., Dijkwel, P. P., Quesada, V., Henderson, I. and Dean, C. (2003). FY is an RNA 3′ end-processing factor that interacts with FCA to control the Arabidopsis floral transition. *Cell* **113**, 777-787.
Smith, T. F., Gaitatzes, C., Saxena, K. and Neer, E. J. (1999). The WD repeat: a common architecture for diverse functions. *Trends Biochem. Sci.* **24**, 181-185.
Takagaki, Y. and Manley, J. L. (1998). Levels of polyadenylation factor CstF-64 control IgM heavy chain mRNA accumulation and other events associated with B cell differentiation. *Mol. Cell* **2**, 761-771.

Wadsworth, W. G. (2002). Moving around in a worm: netrin UNC-6 and circumferential axon guidance in C. elegans. *Trends Neurosci.* **25**, 423-429.
Wang, E. T., Sandberg, R., Luo, S., Khrebtukova, I., Zhang, L., Mayr, C., Kingsmore, S. F., Schroth, G. P. and Burge, C. B. (2008). Alternative isoform regulation in human tissue transcriptomes. *Nature* **456**, 470-476.
Wang, L., Eckmann, C. R., Kadyk, L. C., Wickens, M. and Kimble, J. (2002). A regulatory cytoplasmic poly(A) polymerase in Caenorhabditis elegans. *Nature* **419**, 312-316.
Wang, Q. and Wadsworth, W. G. (2002). The C domain of netrin UNC-6 silences calcium/calmodulin-dependent protein kinase- and diacylglycerol-dependent axon branching in Caenorhabditis elegans. *J. Neurosci.* **22**, 2274-2282.
Wang, S. W., Asakawa, K., Win, T. Z., Toda, T. and Norbury, C. J. (2005). Inactivation of the pre-mRNA cleavage and polyadenylation factor Pfs2 in fission yeast causes lethal cell cycle defects. *Mol. Cell. Biol.* **25**, 2288-2296.
Wang, Y., Gracheva, E. O., Richmond, J., Kawano, T., Couto, J. M., Calarco, J. A., Vijayaratnam, V., Jin, Y. and Zhen, M. (2006). The C2H2 zinc-finger protein SYD-9 is a putative posttranscriptional regulator for synaptic transmission. *Proc. Natl. Acad. Sci. USA* **103**, 10450-10455.
Weimer, R. M., Richmond, J. E., Davis, W. S., Hadwiger, G., Nonet, M. L. and Jorgensen, E. M. (2003). Defects in synaptic vesicle docking in unc-18 mutants. *Nat. Neurosci.* **6**, 1023-1030.
Weimer, R. M., Gracheva, E. O., Meyrignac, O., Miller, K. G., Richmond, J. E. and Bessereau, J. L. (2006). UNC-13 and UNC-10/rim localize synaptic vesicles to specific membrane domains. *J. Neurosci.* **26**, 8040-8047.
Wicks, S. R., Yeh, R. T., Gish, W. R., Waterston, R. H. and Plasterk, R. H. (2001). Rapid gene mapping in Caenorhabditis elegans using a high density polymorphism map. *Nat. Genet.* **28**, 160-164.
Withee, J., Galligan, B., Hawkins, N. and Garriga, G. (2004). Caenorhabditis elegans WASP and Ena/VASP proteins play compensatory roles in morphogenesis and neuronal cell migration. *Genetics* **167**, 1165-1176.
Xu, R., Zhao, H., Dinkins, R. D., Cheng, X., Carberry, G. and Li, Q. Q. (2006). The 73 kD subunit of the cleavage and polyadenylation specificity factor (CPSF) complex affects reproductive development in Arabidopsis. *Plant Mol. Biol.* **61**, 799-815.
Yu, T. W., Hao, J. C., Lim, W., Tessier-Lavigne, M. and Bargmann, C. I. (2002). Shared receptors in axon guidance: SAX-3/Robo signals via UNC-34/Enabled and a Netrin-independent UNC-40/DCC function. *Nat. Neurosci.* **5**, 1147-1154.
Zhang, H., Lee, J. Y. and Tian, B. (2005). Biased alternative polyadenylation in human tissues. *Genome Biol.* **6**, R100.
Zhao, J., Hyman, L. and Moore, C. (1999). Formation of mRNA 3′ ends in eukaryotes: mechanism, regulation, and interrelationships with other steps in mRNA synthesis. *Microbiol. Mol. Biol. Rev.* **63**, 405-445.
Zhen, M. and Jin, Y. (1999). The liprin protein SYD-2 regulates the differentiation of presynaptic termini in C. elegans. *Nature* **401**, 371-375.
Zhen, M., Huang, X., Bamber, B. and Jin, Y. (2000). Regulation of presynaptic terminal organization by *C. elegans* RPM-1, a putative guanine nucleotide exchanger with a RING-H2 finger domain. *Neuron* **26**, 331-343.

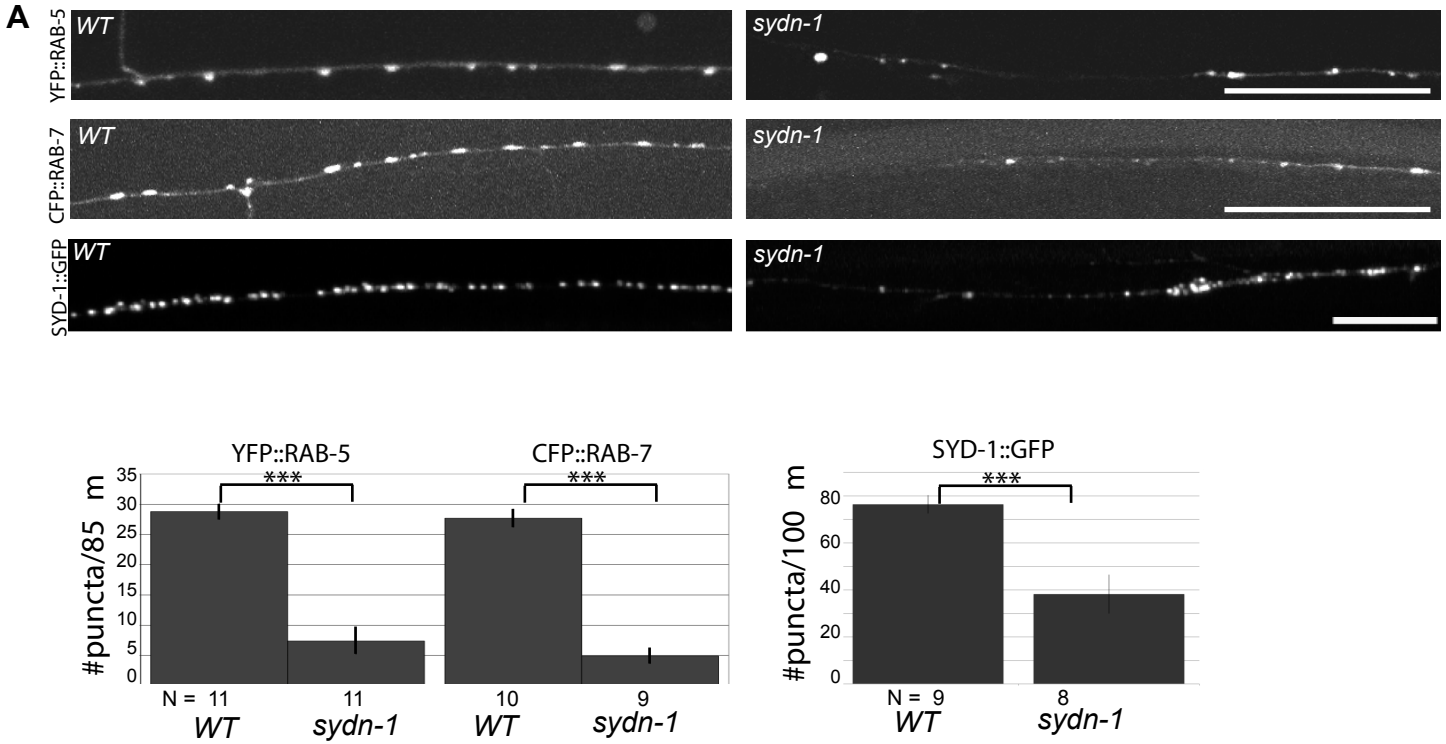
A
YFP::RAB-5
CFP::RAB-7
SYD-1::GFP
WT
sydn-1
YFP::RAB-5
CFP::RAB-7
#puncta/85 m
***
N = 11
11
10
9
WT
sydn-1
SYD-1::GFP
#puncta/100 m
N = 9
8
B
L1
$P_{unc-25}GFP$
sydn-1;syd-2
% Ectopic Branches
L1
1 day adult
8 day adult
N=36
51
11
14
102
20
132
syd-2
26
34
15

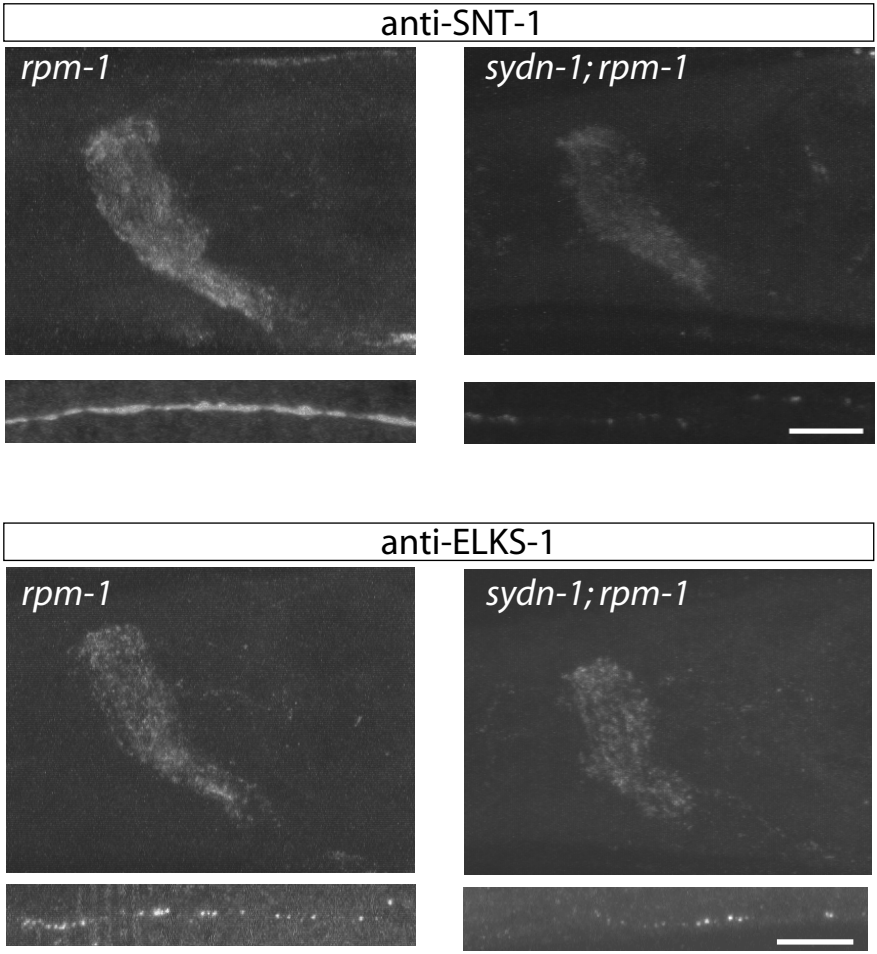
anti-SNT-1
rpm-1
sydn-1; rpm-1
anti-ELKS-1
rpm-1
sydn-1; rpm-1

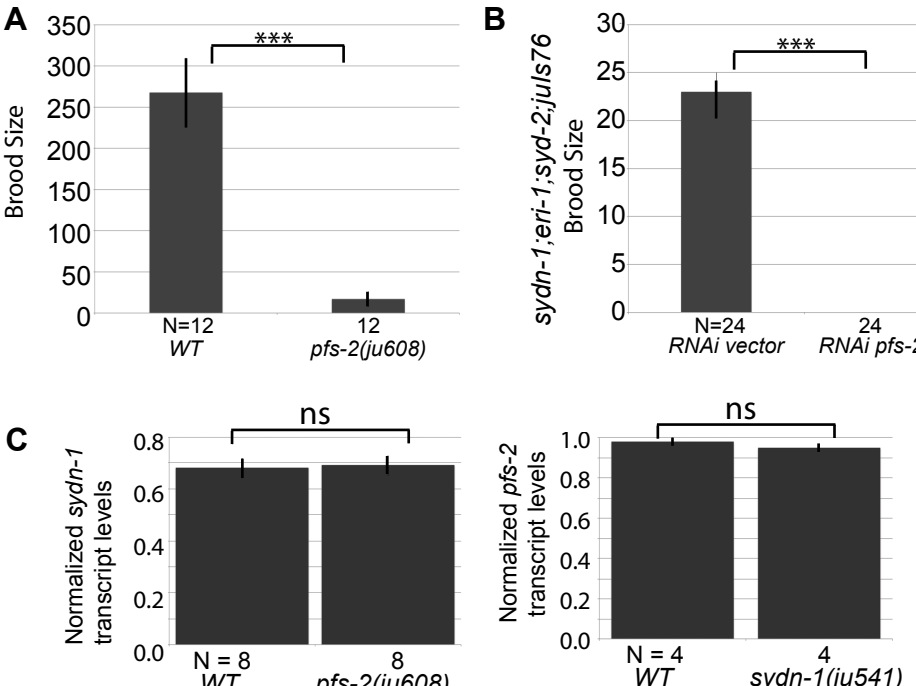
A
Brood Size
350
300
250
200
150
100
50
0
***
N=12
WT
12
pfs-2(ju608)
B
sydn-1;eri-1;syd-2;juIs76
Brood Size
30
25
20
15
10
5
0
***
N=24
RNAi vector
24
RNAi pfs-2
C
Normalized sydn-1
transcript levels
0.8
0.6
0.4
0.2
0.0
ns
N = 8
WT
8
pfs-2(ju608)
Normalized pfs-2
transcript levels
1.0
0.8
0.6
0.4
0.2
0.0
ns
N = 4
WT
4
sydn-1(ju541)

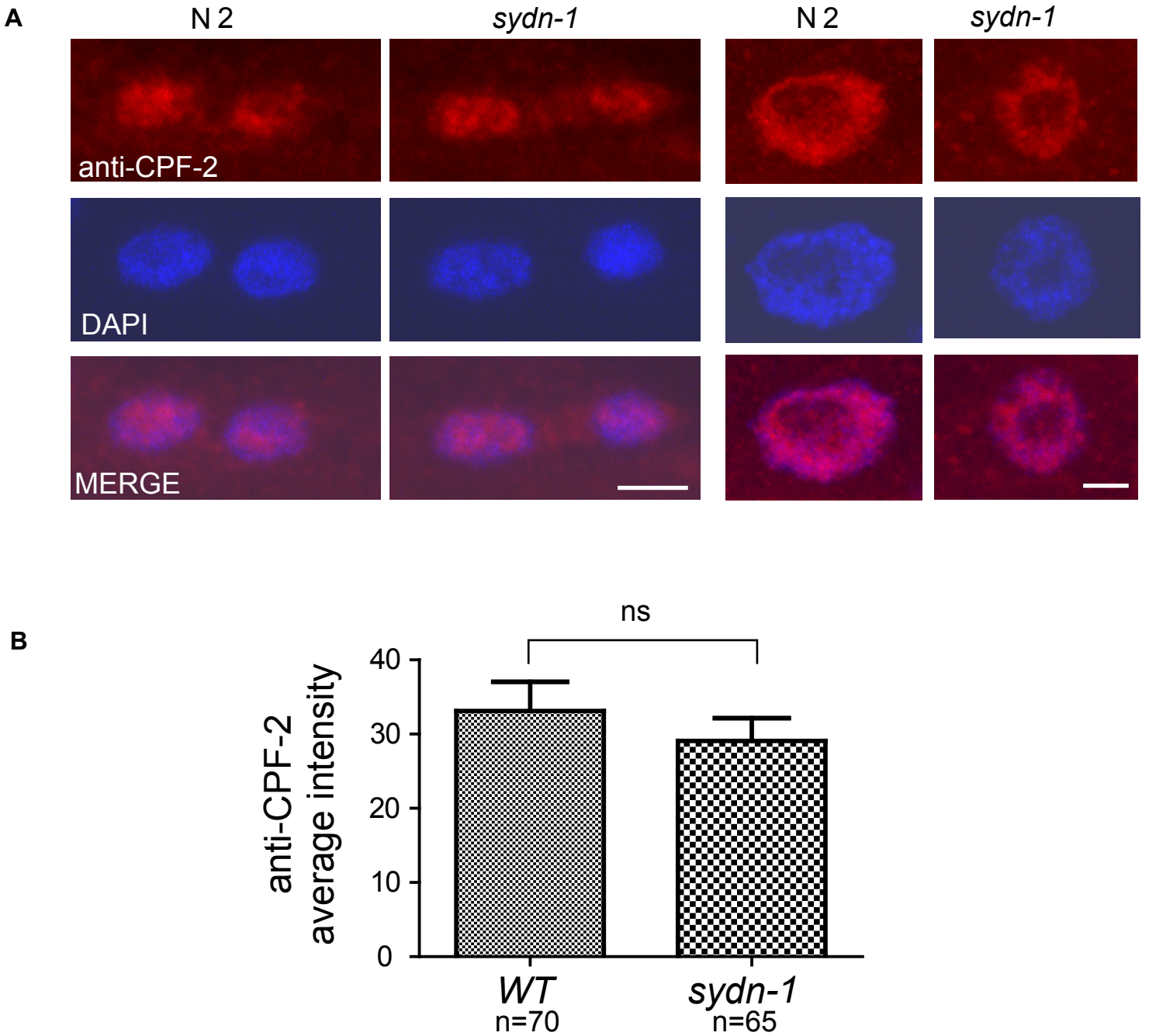
A
N 2
sydn-1
N 2
sydn-1
anti-CPF-2
DAPI
MERGE
B
ns
anti-CPF-2
average intensity
40
30
20
10
0
WT
n=70
sydn-1
n=65

Table S1. List of primers

Gene	Primer	Sequence	Purpose
ama-1	YJ5268	TGCATGGCTCATACGAGAAG	Controls for RT-PCR to test transcript levels
	YJ5269	TGGAAGAAGAATTCCGATGG	"
lin-15A	WW14	ATGCCCTAGCGATGAAGTT	RT-PCR to test transcript levels
	WW15	CATTGGAGTTTGGCTCTCTTT	"
pfs-2	YJ5258	TCCCTGCAGATTCAACTCCT	*ju608* mutation detection; RT-PCR to test transcript levels
	YJ5259	TCGCGATCAGACCTTTTGT	"
	YJ5260	GCCGGACACATTTATTCCTG	RNAi clone
	YJ5266	TTGCCATCCTCCTTGATTTC	"
	YJ5262	CGAGCGCTGGATTTAAAGTTTGTGG	Full-length amplification for transgenes
	YJ5267	CTTGTTCTTCTTTGCTCGAGATGAC	"
	YJ5415	CAGGAAGGCAAAATGCCGC	*pfs-2* GFP
	YJ5416	TTATTATAGAGTCGAATCAGTTGTCATCATGTT	"
sydn-1	YJ3166	GACCCTTTCTGGCAAATCG	*ju541* deletion genotyping
	YJ3167	GGATTCTCTAATTCATTGATATTCC	"
	YJ3175	ATCAGTTGAGACACAGAGCGG	Full-length transgenic rescue
	YJ3728	ACAGCAATATAGAGACAGCCAGG	"
	YJ4563	CGCTACGAGACCCATCTTG	PCR for cDNA determination
	YJ4566	TTGCCATCCTCCTTGATTTC	"
	YJ3169	CAGGGGATGGTTGACAAGC	RT-PCR to test transcript levels; *ju541* deletion genotyping
	YJ3176	GATAGACGGATTCTGATTCGG	RT-PCR to test transcript levels
	YJ5422	TTATCGGATCAAATGGAGCTG	"
	YJ5423	TGCTGATATAACCCCTGCTG	"
	YJ5270	GGCTCCGTATCAGCACCAGG	"
	YJ5271	TAAGGAGGTGGCTGAATTGG	"
SP1	YJ4041	GATAACTACCACCATCAGAATCG	5′ RACE *sydn-1*
SP2	YJ4040	TTCTCGTAGCCCAGCGTC	"
SP3	YJ4039	ATTTGTCGCAGTCAATGGC	"
SP5	YJ4171	ATGGCTCCGTATCAGCACCAG	3′ RACE *sydn-1*